

Final Response Form

Dear Editor,

We have responded to the interactive discussion of RC1, RC2 and RC3 one by one, and the response to the editorial corrections.

The following is the final form of the reply.

Thank you much for your kind help!

Fei Hu

Yu Shi

1. Response to RC 1

Dear reviewer,

Thank you very much for your comment on our paper, we think it is really very valuable and it helps us a lot.

In particular, as the first author, I am currently a Ph.D. student. I have really learned a lot of boundary layer knowledge from your comments. I would like to express my respect and heartfelt thanks to you!

Based on your review comments, we have added some calculations, redrawn some of the figures, and responded to your comments one by one in the attachment, and adopted all your suggestions. Specifically:

- 1) Complement all recommended references.
- 2) Added MODIS satellite cloud image.
- 3) Corrected the representation of the height of the radiosonde detection boundary

layer. As you said, the maximum temperature gradient method we obtained should be the residual layer top height.

4) Recalculating and drawing with high-resolution radiosonde, giving the wind profile of the low-level jet during heavy pollution. As you pointed out, we should use the jet height (or low-level wind extreme) as the boundary layer height. The value of the boundary height has also been corrected. The drawing is shown in Figure 6.

5) Increased the daily variation of the surface wind field in Beijing and the discussion of the removal of pollutants by cold air.

6) Respond to all major and minor comments you have given.

7) Carefully revised and edited the full text of the paper, and many details were rewritten.

Thank you very much !

Yours sincerely,

Yu Shi (first author)

Fei Hu (corresponding author)

● **Response to the Major comments**

Major comments (a) : In Sect. 3.3, the authors use the maximum gradient in the potential temperature to identify the PBLH in radiosonde data. This method is only appropriate in the convective PBL (as in the cited Hennemuth and Lammert, 2006 study). Based on the profiles shown in Fig. 4, the PBL was stable and this method is inappropriate to determine the PBLH. Seidel et al (2010) further discusses how the PBLH should be determined in a SBL and the problems of using the maximum gradient in potential temperature in these conditions. It's also important that the authors clarify what they mean by the PBL height. Is the layer that is currently being mixed as it interacts with the surface the desired layer? This is often very shallow in the SBL. Alternatively, do the authors mean the height of the residual layer (from the previous day's CBL)? If the later is the case, then the potential temperature method may be appropriate. However, it must be noted that this height (top of residual layer) is not where pollutants are actively mixed, which is the desired quantity for air pollution studies. See also Keller et al (2011) for a method in which the SBL height can be calculated from a temperature profile.

Response: The maximum temperature gradient method we used is indeed inaccurate and is affected by the depth of residual layer. In the revised paper, we discussed and revised this point and gave relevant references. On the other hand, the radiosonde data we used was obtained at 08:00 and 20:00 local time, and they are not the typical time period of the nighttime boundary layer and convective boundary layer, because the sunrise and sunset time in winter in Beijing is about 07: 00 and 19:00. Therefore, it is necessary to make a concrete analysis in view of different potential temperature profiles. The expression of "maximum potential temperature gradient method" in the first draft is indeed inappropriate, because of the influence of surface inversion and residual layer. As Seidel pointed out (Seidel et al., 2010), the vertical resolution of radiosonde data will affect the estimation of boundary layer height. So in the revised version, we collected and used more high-resolution radiosonde data.

As for the definition of inversion layer and residual layer, we also added in the introduction as follows:

Because of the Earth's rotation, the ABL presents strong diurnal variation, leading to the formation of many different layers in the boundary layer. The mixing layer accounts for a large proportion of the ABL in the deep convective boundary layer, and at present, the height of the mixing layer is equivalent to the height of the ABL. Pollutants emitted into the ABL can reach a certain height through turbulent vertical mixing processes (Emeis and Schäfer, 2006), making it possible to determine the ABL height from the concentration of pollutants. The top of the mixing layer exhibits capping inversion. Due to a change in the surface net radiation occurring at night, a stable boundary layer begins to form at night because of the cooling effect of the ground surface, and the surface inversion layer is nearest to the ground. The nocturnal stable boundary layer is often accompanied by a residual layer that maintains the characteristics of the daytime mixing layer (Stull, 1988).” (Page2 line7-15, in the revised paper)

The maximum potential temperature gradient of the first draft is indeed affected by the residual layer, which often appears bigger potential temperature gradient. At 08:00, there are often no obvious potential temperature gradients (For example 08:00 18 December, seen fig1). When the inversion layer caused by surface cooling is significant, there is the obvious change of potential temperature gradient, which can be regarded as the stable boundary layer height.

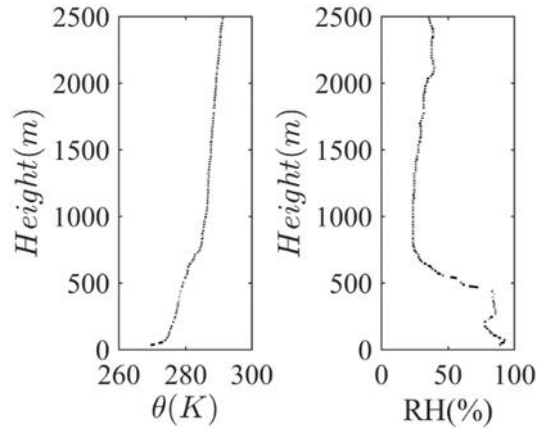


Fig. 1 Profiles of potential temperature and relative humidity at 08:00 18 December

In the revised paper Fig5.a b c (seen fig.2), PBL height can be determined by potential temperature gradient method. For Fig5b, besides the surface inversion on the ground, the height where potential temperature gradient reaches maximum is about 1000m, and there is also an obvious change of potential temperature gradient at 600m. At this time, combined with the change of relative humidity profile, the height of boundary layer is determined to be 680m by comprehensive analysis.

Therefore, in the revised version, the expression of the determining the boundary layer height by radiosonde is changed to:

“In this study, the level showing an obvious change in the potential temperature gradient and the profile of relative humidity were used to define the ABL height, as expressed by H_θ ” (Page11, line13-14, in the revised paper)

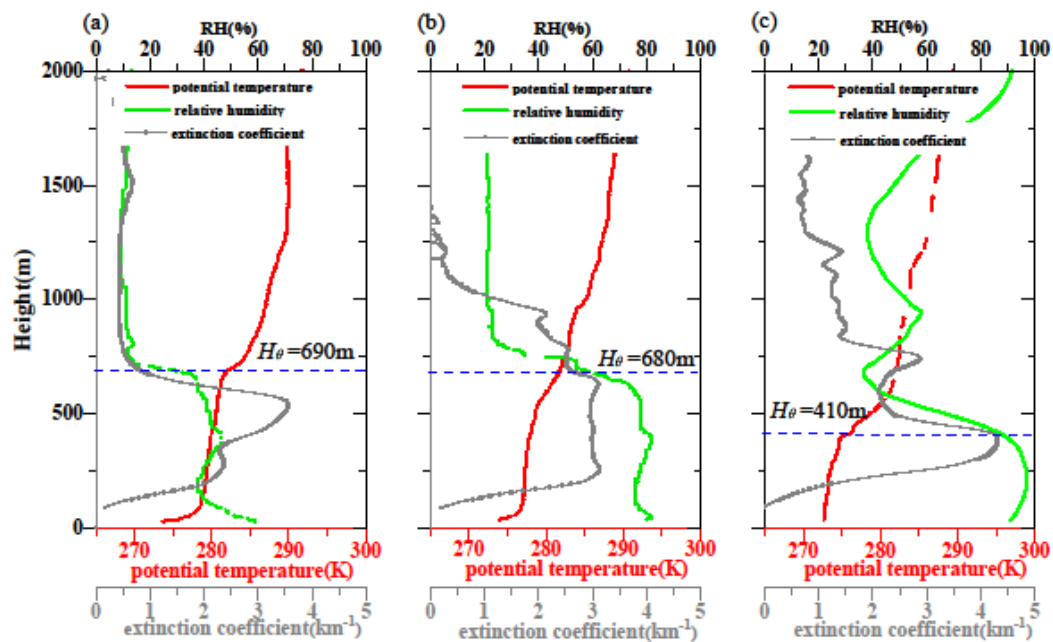


Fig. 2 (Figure 5 in the revise paper)

Refernce:

Seidel D J , Ao C O , Li K . *Estimating climatological planetary boundary layer heights from radiosonde observations: Comparison of methods and uncertainty analysis[J]. Journal of Geophysical Research Atmospheres, 2010, 115(D16), doi: 10.1029/2009JD013680.*

Major comments (b): In Sect. 3.4, the authors identify the PBLH as the maximum in the wind speed. While this method has been used before (as the authors note in the cited studies), it is only appropriate for identifying the PBLH when a low-level jet is present, which there is not during much of this study. Instead, the authors should use a more appropriate method for determining the PBLH from a WPR, such as Cohn and Angevine (2000) or Bianco et al (2002). It important to consider that WPR are often currently unable to measure the PBL height in the stable boundary layer due to the PBL being shallow (below the minimum range gate) and there is rarely a refractive index maximum signature. If a different more appropriate method is not used, then the WPR PBL height measurements should be removed from this study.

Response: According to the opinions of the reviewers, this maximum wind value can only be applied in the case of low-level jet structure, so we reanalyzed all the wind profiles of this process, and selected the profiles that have obvious “nose” structure or have reached the standard of low-level jet, so as to determine the PBL heights under this kind of wind profile. Here, we give the wind profiles of December 15, 17, 19 and 21 (all are local station time, seen fig.3). Although some cases did not meet the LLJ standard at some moments, it also had obvious “nose” structure. Below the height of the low level wind maximum is where affected by the ground friction, it can be concluded that the height of the low level wind extreme value at this time is the boundary layer height. The wind profiler radar can output the atmospheric refractive index structure parameter and determine the height of the boundary layer based on it. It is difficult to detect the stable boundary layer height because of the weak turbulence, so the boundary layer height based on refractive index structure parameter is mostly used in the convective boundary layer (Heo et al., 2002). However, atmospheric refractive index structure parameter was not used in this paper. Instead, wind profiles detected by WPR were used in this paper we, therefore, we still keep the results of wind profiler radar data, and gives the analysis results of the wind structure from low to high levels during the period of urban heavy pollution period.

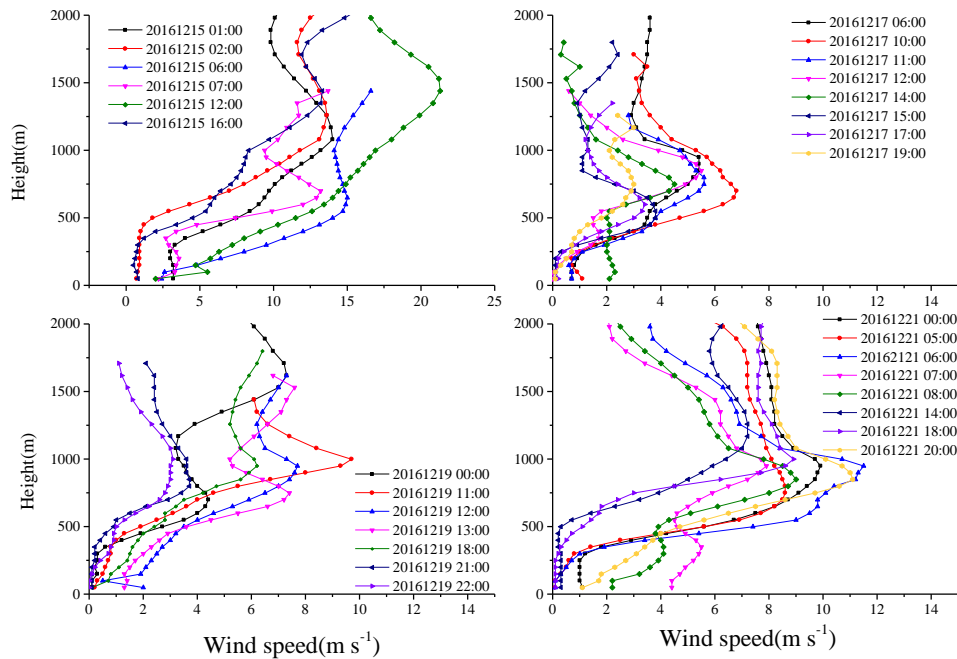


Fig. 3 Wind profiles of December 15、17、19 and 21 (Figure 6 in the revised paper)

Reference:

Heo B H , Jacoby-Koaly S , Kim K E , et al. Use of the Doppler Spectral Width to Improve the Estimation of the Convective Boundary Layer Height from UHF Wind Profiler Observations[J]. *Journal of Atmospheric and Oceanic Technology*, 2003, 20(3):408-424.

Major comments (c) : This study could benefit from a discussion of the synoptic and mesoscale meteorology. Based on Fig. 2, it looks like there were cold fronts (strong NW winds) on both 12/15 and 12/22 which advected pollutants away and resulted in air quality. Between the fronts, the PM_{2.5} slowly increased as the air was stagnant (weak and variables winds in between) and pollutants emitted locally likely slowly built up. The wind direction also seems to be cyclical every day, perhaps this is in response to a local mountain-valley circulation around Beijing? This warrants more investigation. It appears that these factors, namely the stagnant air, dominate over the PBL processes in resulting in the poor air quality.

Response: We fully agree with the reviewer's analysis and added a paragraph and a reference to the revised paper as follows:

“From Fig. 2, we can see that there were cold fronts (strong NW winds) on both 15 December and 22 December, which advected pollutants away, resulting in good air quality. Between the fronts, PM_{2.5} levels slowly increased, as the air was stagnant (weak and variable winds in between), and the pollutants that were emitted locally slowly built up. The wind direction also seemed to be cyclical on each day in response to local mountain valley circulation around Beijing (Hu et al., 2005).” (Page6 line17-20, in the revised paper)

Major comments (d): While the authors provide numerous references early in the manuscript, there is little-to-no discussion of how the key findings and results compare to previous studies. For example, how does this haze episode compare to other poor air quality case studies in Beijing and other areas, considering both meteorology and boundary-layer processes? The authors should relate the hygroscopic growth to that observed in other studies (there are many). There have also been many other studies comparing lidar PBL heights with those from radiosonde and/or wind profilers, mainly focused on the convective boundary-layer where the top of the boundary-layer is clearly defined. These studies should be related to as well.

Response: The main purpose of this paper is to analyze characteristics of boundary layer structure during a red warning haze episode in Beijing, such a typical mega city, from the direct observation (radiosonde and tower) and remote sensing (lidar and wind profiler radar). We adopt the reviewer's opinions and analyzed the boundary layer height determined by lidar, radiosonde and wind profile radar in the polluted period. Therefore, the previous literatures on the boundary layer height have been added to the introduction. We also pointed out the shortcomings of previous studies and pointed out the relationship between this paper and some related studies in the revised paper:

“The ABL height is closely related to air pollution, but it is not the only factor that shapes air quality. Pollution conditions are also affected by wind speeds, emissions, chemical processing, etc. (Schäfer et al., 2006; Geiß et al., 2017). Some works have compared ABL heights based on lidar and radiosonde data, and the correlations between them are stronger under unstable conditions (Emeis and Schäfer, 2006; Martucci, et al., 2007). However, for ABL heights determined from wind, relatively fewer studies have compared and analyzed the results of lidar and radiosonde tests applied during haze pollution episodes.” (Page2 line15-20, in the revised paper)

“The Lidar results overestimate the ABL height at night (Quan et al., 2013). In this study the ABL height also increased due to the accumulation of pollutants during the period of heavy pollution.” (Page18 line5-7, in the revised paper)

Reference:

Schäfer K , Emeis S , Hoffmann H , et al. Influence of mixing layer height upon air pollution in urban and sub-urban areas[J]. *Meteorologische Zeitschrift*, 2006, 15(6):647-658.

Alexander Geiß Wiegner M , Bonn B , et al. Mixing layer height as an indicator for urban air quality?[J]. *Atmospheric Measurement Techniques*, 2017, 10(8):2969-2988.

Emeis S , Schäfer K . Remote Sensing Methods to Investigate Boundary-layer Structures relevant to Air Pollution in Cities[J]. *Boundary-Layer Meteorology*, 2006, 121(2):377-385.

Martucci G , Matthey R , Mitev V , et al. Comparison between Backscatter Lidar and Radiosonde Measurements of the Diurnal and Nocturnal Stratification in the Lower Troposphere[J]. *Journal of Atmospheric & Oceanic Technology*, 2006, 24(7):1158-1164.

● Response to the Minor comments

a) P. 1 line 13: ‘Turbulent activities were great inhibited during haze pollution’. This must be rephrased, as the evidence in the paper does not support this statement. It is unclear if the haze suppresses turbulence, or if weak turbulence results in poorer air quality.

Response: Indeed, whether the turbulence affects pollutants or pollutants affects turbulence, the evidence in this paper is not very clear. This sentence has been changed to:

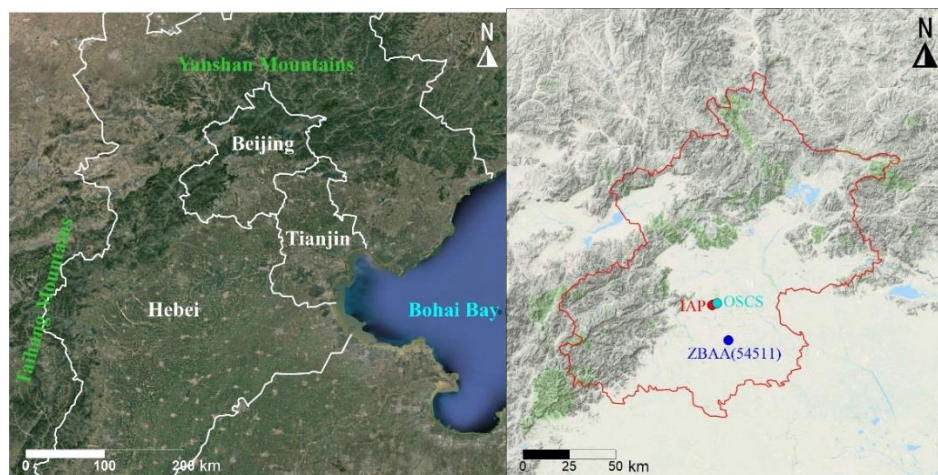
“Turbulence and pollutant concentrations are closely related during periods of haze pollution”.
(Page1 line14, in the revised paper)

b) P. 2, line 8: ‘Please define all the acronyms, such as for URBAN, MIAGE, and SURF (similarly to how COST was defined and spelled out)’.

Response: The explanation of these abbreviations nouns is added in the revised paper.
(Page.2 line22-27, in the revised paper)

c) Figure 1: Add a reference scale for distance on the plot. Currently, this map is not very informative in itself. It would be beneficial to add other details to the map relevant to the study (i.e., other important locations, elevation map, any significant pollutant sources, etc) if possible.

Response: We have redrawn this figure to make it more standard. First, the topographic map of Beijing and its surrounding areas have been added, and some important details have been added to the map, and the scale has been added. As shown in the Figure1, we marked the mountains, bays and other topography around Beijing, and marked the observation data during this period. In figure4, the east of Beijing is the Bohai Bay, so generally the easterly wind will bring water vapor to the Beijing area, which can help to explain some characteristics.



(a)

(b)

Fig. 4 (Figure 1 in the revised paper) Local topography of Beijing and of its surrounding area (a).

The locations of observation sites in Beijing (b): red circle: IAP (Lidar), blue circle: ZBAA radiosonde observation station, cyan circle: pollution observation station (OSCS) positioned approximately 2 km northeast of the Lidar. Beijing is a densely populated city covering an area of approximately 396 square kilometers.

d) P. 3 line 14: It is stated there are 15 platforms on the tower, but only 14 levels are subsequently listed. This inconsistency should be rectified.

Response: Thank you very much for your comments, and we are very sorry for this carelessness. We have modified this mistake. (Page4, line3, in the revised paper)

e) P. 4 line 16: List out the six air pollutants measured.

Response: We have listed out six types of pollutants here and modified it in the paper. (Page5, line1, in the revised paper)

f) Table 1: What is the difference between ‘heavy polluted’ and ‘serious polluted’? Describe in the text these categories (and all the other ones). It is unclear which category is worse. These are later defined in Table 2 at the end of the manuscript, but these definitions should be moved to the discussion of table 1.

Response: We have adopted the comment by reviewer, and have moved the definition to the discussion of Table 1. (Page5 table1, in the revised paper)

g) P. 5, line 3: Here, the authors claim that the lack of diurnal variation of temperature and RH is due to heavy pollution. This is plausible, but another reason is more likely. The high RH and low visibility, secondarily combined with the low wind speed, all indicate that fog or low stratus is present. The fog or stratus itself would greatly reduce insolation and daytime heating. This would effect would likely dominate over aerosol effects in reducing solar radiation reaching the surface. The discussion here needs to be modified accordingly. It would also be useful to include a plot of cloud cover somewhere.

Response: Thank you for your help with the modification explanation of the temperature and RH diurnal variation characteristics due to the heavy pollution. We have added the MODIS cloud figures in this paper (Figure.3 in the revised paper), and further analysis of satellite cloud images during this period shows that:

“pollution process was indeed accompanied by fog, while pollution formed in the south-central area of Hebei Province on 15 December 2016 and then spread across the whole Beijing-Tianjin-Hebei area on 18 December. Stratiform clouds appeared in areas surrounding Beijing on 21 December, but due to the high concentrations of pollutants (PM_{2.5} values approaching 400 μg m⁻³, mixed fog and haze appeared in Beijing. During the day, pollutants can

scatter more solar radiation while the ground receives less solar radiation, leading to the suppression of diurnal variations in temperature and relative humidity on the ground. (Page6, line6-11, in the revised paper)

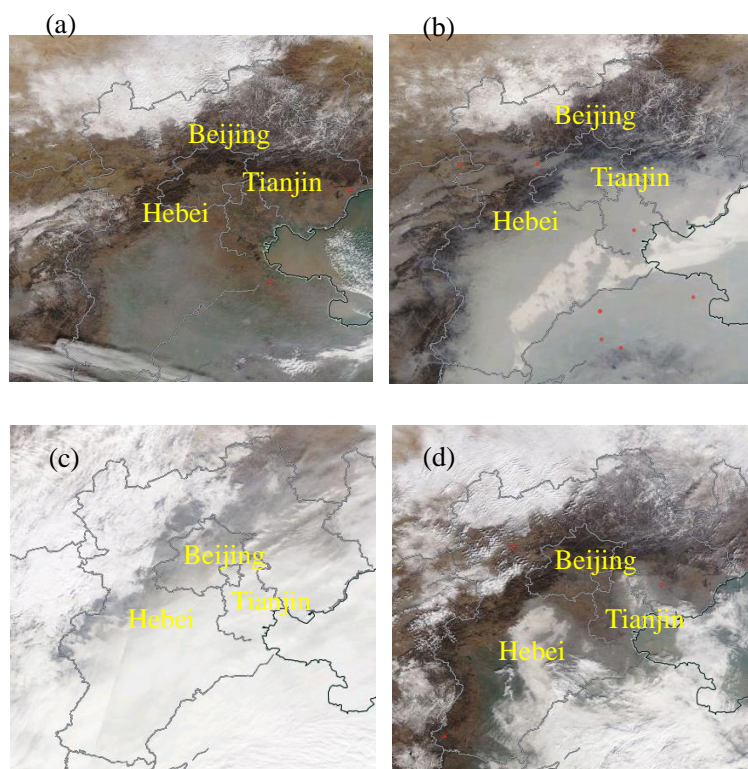


Fig. 5. (Figure. 3 in the revised paper) MODIS image of Beijing-Tian-Hebei area from 14-23 December 2016. (a)15 December 2016, (b)18 December 2016, (c)21 December 2016, (d)22 December 2016

h) P. 5 lines 6-7: RH cannot be used to quantify the total amount of water vapor in the air, as RH is highly-dependent on the temperature. The increase in moisture discussed here may simply be due to a lower temperature, not an increase in water vapor content. Please use mixing ratio or another conserved quantity.

Response: Because relative humidity is dependent on temperature, so that this paper compared relative humidity on the condition of the same temperature. Ground observation data shows that the temperature at 00:00 17 December and 00:00 20 December were all -4°C , but the relative humidity at 00:00 20 December was 100%, far more than it at 00:00 17 December(74%). Since the temperature was the same, we infer that there was an increase in water vapor at 00:00 20 December.

Time	Temperature ($^{\circ}\text{C}$)	RH (%)	Wind speed (m s $^{-1}$)	Wind direction (degree)	Visibility (km)
2016/12/17 00:00	-4	74	2	350	4

i) Sect 3.2: Rename this section “Lidar observed boundary layer heights”, as the WPR and radiosonde and not discussed in it. These paragraph needs to be rewritten and better organized. Start by explaining why the extinction profile can be used to identify the ABL height, then lead into three different methods that can be used that will yield different estimates, but also each have their own limitations. Describe each method separately, as currently the description of all three is spread throughout the entire section.

Response: Thank you for your comment. We have modified it to “Boundary layer heights observed by Lidar”. In addition, we have rewritten this paragraph as follows:

“The most basic definition of the ABL height is the height at which the influence of the Earth's surface on the lower troposphere disappears. This influence applies not only to conventional meteorological elements but also to turbulence quantities and even more for substances in the atmosphere such as aerosols, water vapor and nonreactive tracer gases (Seibert et al., 2000). Levels of various pollutants and water vapor in the ABL are much higher than those found in the free atmosphere, and therefore, there is often an obvious aerosol concentration gradient between the boundary layer and the free atmosphere. The extinction coefficient reflects the degree of aerosol particle scattering from lasers in the atmosphere (Boers and Eloranta, 1986). Thus, the ABL height can also be estimated from the extinction coefficient gradient. We used three popular methods---the gradient method (Lidar_gra) (Flamant et al., 1997), the standard deviation method (Lidar_std) (Hooper and Eloranta, 1986) and the wavelet method (Lidar_wav) (Cohn and Angevine, 2000; Davis et al., 2000; Brooks, 2003) ---to extract boundary layer heights from extinction coefficients. The ABL height determined by Lidar is represented by H_c . In this study, the Lidar_gra method applies the height of the atmosphere at which the gradient of the Lidar extinction coefficient reaches its most negative value. The standard deviation of the extinction coefficient reflects the degree of Lidar echo signal dispersion at different heights. The top of the planetary boundary layer constitutes the intersection between air in the boundary layer and the free atmosphere, which leads to a strong signal change at the top of the boundary layer. We define the height of the maximum standard deviation of signals as the ABL height. The Lidar_wav method can also be used to detect abrupt changes in signals, so we use the Haar wavelet and take the height at which the wavelet coefficient is at its highest value as the height of the ABL. These methods are used

to find the abrupt change in the extinction coefficient occurring at the top of boundary layer, though they present their own limitations.

Generally, the atmospheric boundary layer can be divided into a daytime convective mixing layer and a nighttime stable boundary layer. In the morning, the well-mixed convective boundary layer (CBL) is growing and often reaches its maximum height in the early afternoon. In the afternoon, the CBL gradually transforms into a neutral boundary layer. Figure 4 illustrates the evolution of ABL heights measured with Lidar, WPR and radiosonde tools.”

(Page8-9, in the revised paper)

j) P. 7, line 10: What is the dilation of the Haar wavelet? The determined ABL height

has been shown to be sensitive to this in many previous studies.

Response: The selection of dilation of the Haar wavelet is the key in this wavelet transformation method, and Brooks (2003) proposed that the best selection of dilation parameter a should be equal the transition zone range of the ideal profile. We take $a=6$ as the dilation of continuous Haar wavelet transformation in this paper, and PBL heights calculated based on it coincide with the edge regions where distinct changes of extinction coefficients exist. We have added the following in the revised paper:

“(continuous Haar wavelet transformation was used in this paper, taking dilation paramet $a=6$).”
(Page 8, line 11 in the revised paper)

Reference:

Brooks I M . *Finding Boundary Layer Top: Application of a Wavelet Covariance Transform to Lidar Backscatter Profiles[J]. Journal of Atmospheric and Oceanic Technology, 2003, 20(8):1092--1105.*

k) Figures 3 and 4: Why is extension near the surface so small? I would expect the extinction profile to be nearly uniform (most of the time, except in the presence of clouds) throughout the entire PBL. This leads me to believe that the overlap correction for the lidar is not correctly determined and/or applied. Also, in calculating the extinction coefficient, is attenuation considered? Also, please state if time here (and throughout the manuscript) is local time or GMT.

Response: Mainly because the blind zone of the radar has a thickness of several tens of meters, and the measurement in the near-surface layer is not reliable. We have stated the time used in this paper is local station time in Section2: Observation sites, instruments and data “We use local station time in this work, and the observational instruments and data employed are as follows:.....” (Page3 line28, in the revised paper)

l) P. 8 line 8: What is meant by ‘transformation zone’? This is not a commonly used term. m) P. 8 line 10: This reasoning is insufficient to discount the lidar observations, especially given following concerns with the PBLH determined from both the radiosonde and wind profiler. If the extinction is plotted on a logarithmic scale (which is more appropriate given the large dynamic range that it can vary), a real gradient associated with the PBLH determined by the lidar would likely be more apparent. Hints of this gradient are apparent on the plot now during these clean periods at around 250m on 12/15 and 12/22.

Response: thanks to the reviewer, “transformation zone” should be “transition zone”, and have rewritten this expression into:

“the aerosol concentration was low and the extinction coefficient derived from the Lidar system

displayed no obvious signs of decline from the ground to the upper height” (Page10, line8-9, in the revised paper).

In this paper, the extinction coefficient is lower and the height where holding big extinction coefficient gradient is relatively low of clean days.

n) P. 8, line 23: The fact that the PBL was statically stable is unsurprising given the timing of the radiosonde profiles at 08:00 and 20:00 local time, which are respectively about 30 min after sunrise and 3 hours after sunset during the experimental period. Thus, a nocturnal inversion would barely erode by 08:00 (if at all, depending on the energy balance as insolation is small) and a nocturnal inversion would have formed by 20:00. Due to the timing, these profiles are not representative of conditions during the day when pollutants are actively mixed. I suspect that if the profiles were during the midday (noon local time or early afternoon) the profiles would indicate instability and mixing. This must be discussed at the very least.

Response: Thank you for the comments pointed out by the reviewers, we adopted this discussion in the text. However, due to the limitation of radiosonde in Beijing, only profiles at 08:00 and 20:00 are available. By adding the observation profiles of the daytime of the tower, the typical convective or nocturnal boundary layer characteristics are only analyzed by means of the tower observation.

o) P. 8, line 28-29: Based on this description (and the profiles), it seems as though the top of the stable boundary layer where mixing is occurring is at 100 m (not 700 m), while the top of the decoupled residual layer is at 700 m.

Response: Thanks to the reviewer for pointing out our mistakes, At this time, the potential temperature between 100-600m is not almost unchanged, or it shows an obvious inversion layer, so we revised the relevant expression in the paper:

“Due to the cooling effects of surface longwave radiation, the ground inversion layer frmed from the surface at a depth of approximately 100 m. At this time, the potential temperature gradient underwent an obvious change at 600 m. The inversion intensity levels below 600 m was weaker, and the height Htheta was approximately 690m.” (Page11, line30-32, in the revised paper)

p) P.9, line 5: Why would an easterly wind advect water vapor? This is unclear and not supported by the data. A map of the water vapor field at the time would be needed to support this.

Response: Thank the reviewers for their comments. It is indeed our negligence. By giving topographic map (Figure1 in the revised paper), it can be seen that the east part of Beijing is the Bohai Bay. Generally, the easterly wind, especially the southeast wind, can bring abundant water vapor to Beijing.

q) P. 9 line 6: The authors should provide a reference here for hygroscopic growth, as it has been detailed in numerous prior studies.

Response: P.9 line6: According to the reviewer's suggestion, here we have added 3 references: Svenningsson et al. (1992), Chuan (2003) and Pan et al. (2009).

r) P. 9 line 8: The profile still appears stable in panel c) as the inversion is not completely eroded yet with potential temperature increasing from the surface upwards, thus the ground inversion is still apparent (although weaker) than in panels a) and b).

Response: We adopted this discussion and we have deleted the expression “The ground inversion layer has disappeared” .

s) P. 9 line 11: Why is H_{θ} at 604m? By eye, the maximum in the gradient of the potential temperature (and humidity) is near 350 m.

Response: Initially, because of the low vertical resolution of our radiosonde data. Based on the reviewer's opinion, we used the high vertical resolution radiosonde data and the new calculated H_{θ} was about 410m. (Page12, line12, in the revised paper)

t) Figure 4: The tick marks on the right-most y-axis in panel c) are not aligned with all the other tick marks, which is confusing and deceptive. Also, why do all the profiles start at around 50 m? Is this height above ground level or height above sea level?

Response: We redrew Figure4 (Figure.5 in the revised paper) and made sure that the tick marks on the right-most y-axis in panel c) are aligned with the other tick marks. The height is above the ground level, and first sounding data is basically from 30m.

u) P. 9 line 13: Rephrase the sentence “At the inversion layer, it was easier to appear the larger value of the potential temperature gradient”, as its meaning is unclear.

Response: we have rewritten this sentence and made it more clear:

The potential temperature gradient at the inversion layer is generally larger. (Page12, line16, in the revised paper)

v) P. 9 line 16: Again, please provide evidence to support this statement. Perhaps in Fig. 4 a few panels could be added (and a supporting discussion in the text) that show profiles where there is no inversion layer apparent (or it is weak).

Response: According to the reviewer's opinion, considering that this paper is only a case study of one air pollution process, there is not enough evidence to support the sentence “However, when the atmosphere was clean, the aerosol concentration was obviously reduced and the inversion layer was not so significant.”, so we remove this sentence in the text.

w) P. 11 line 4: The equation for u_*' is incorrect. The $u'w'$ and $v'w'$ quantities should both be squared. Make sure it is calculated correctly in Fig. 6, b as well.

Response: The calculation of friction velocity in Fig. 6 is corrected. Thank you for your reminder. We revised the expression of friction velocity correctly. (Page15 line5, in the revised paper)

x) Fig. 7: Please make the colorbar for the wind direction (in leftmost panel) circular. With the current colorscale, wind direction at 359 deg is red and 1 deg is blue, even though there's little difference in the wind direction. It would also be beneficial to provide plots from daytime conditions when the PBL is well-mixed during the pollution episode, as both of the selected time periods are near midnight

Response: Based on your comments, we have redrawn these figures to make the wind direction clear, and have deleted the description of $\overline{w'^3}$ and added the plots from daytime comparison between clear and pollution day. (Figure9 and Figure10 in the revised paper):

“In the daytime on 21 December 2016 (see Fig. 10), the $PM_{2.5}$ concentrations reached roughly $400 \mu g m^{-3}$, wind speeds were low, TKE remained zero value, and the potential temperature observed from the tower during the period of pollution basically denoted neutral stratification. The sensible heat flux was positive, but the value was basically measured as $0.02 K m s^{-1}$. At noon on 22 December, when the weather had improved, wind speeds were clearly higher. TKE still reached a maximum at 47 m. The influence of the urban canopy was stronger at heights of below 47 m. Unlike on the polluted day, levels of sensible heat flux were higher at this time, and the lower layer reached a value of $0.1 K m s^{-1}$. The tower observation data clearly show that levels of sensible heat flux decreased significantly in the daytime during the haze episode because of the higher levels of solar radiation scattering by particles.” (Page17 line1-8, in the revised paper)

y) Table 2 (and its discussion): There appears to be little difference between slightly, moderately, heavily, and seriously polluted conditions. There is no clear trend in the listed variables with increasing pollution. I suspect that the calculated small differences are not statistically different between categories, except compared with ‘good’ air quality. This is unsurprising, given the meteorology remains roughly constant during all periods between times when the air quality is ‘good’ when pollutants slowly build up. This should be discussed

Response: Thanks to the reviewer for his valuable comments, we use the ABL height “heightened slightly”, and added a sentence in the text:

“Since the data examined in this study apply to only one period of heavy pollution, the minor differences observed may not be statistically different across categories except when compared to “good” air quality conditions.” (Page18, line 10-11, in the revised paper)

z) P. 15 line 6: Again, there is no evidence in the manuscript that north-easterly winds brought pollutants and water vapor to Beijing. Based on Fig. 2, it looks like this first increase in pollution was the first night when winds were light, thus pollutants likely

emitted locally were not dispersed and built up quickly in a shallow layer near the surface.

Response: P.15 line6: Thank the reviewers for their comments. At first, we analyzed the 10m wind field data from FNL reanalysis data. The convergence zone of northeast and southeast winds in the east part of Beijing is shown in the yellow dotted line frame. Later, the 10m wind field data map was not added due to the use of ground observation data and wind profile radar. So, we revised the relevant expression in the paper.

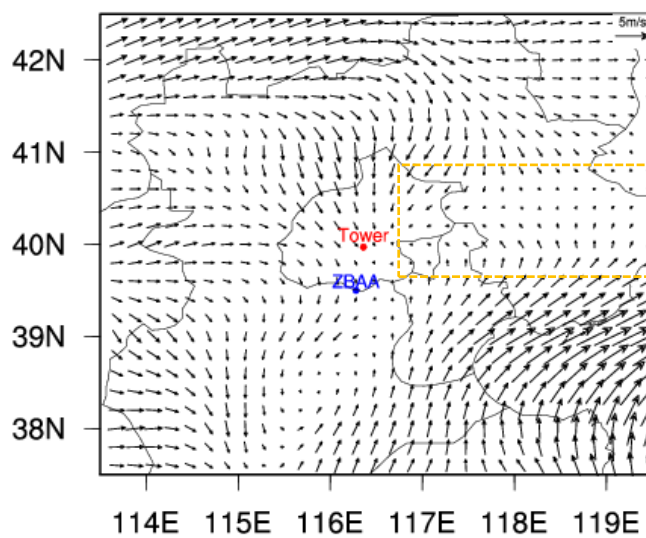


Fig.6.10m wind field from FNL reanalysis data (08:00 17 December)

aa) P. 15 line 13: Rephrase the sentence ‘The turbulent fluxes...radiation from the ground’, as its meaning is unclear

Response: Based on your comment, we have rewritten this sentence to make it clear “Turbulent fluxes varied very little with altitude, but the sensible heat flux measured at night was slightly positive close to the Earth’s surface, indicating that the cooling effect is inhibited by long-wave radiation from the ground.” (Page20 line15-17, in the revised paper)

bb) P. 15 line 15: How is turbulence suppressed when the sensible heat flux is positive? Normally a negative heat flux with cooling near the surface will strengthen the stability limiting turbulence, while a positive heat flux weakens stability

Response: Yes, our high-resolution 7-layer turbulence instrument observation shows that the sensible heat flux on the ground was positive at night during the pollution period. First of all, at night, due to the presence of pollutants and more vapor, the long-wave radiation cooling effect from the ground was inhibited. Furthermore, in a city with large population, such as Beijing, the building heat storage and anthropogenic heat of the city also made it possible that the surface sensible heat flux

appeared positive at night.

2. Response to RC2

Response to the RC2

Comments:

The authors have addressed my comments satisfactorily. I think the manuscript is acceptable for the publication.

Response:

Thank you very much for your positive comments on our paper and think it is acceptable for publication. The revised paper was sent to you as an attachment.

3. Response to RC3

Dear reviewer,

Thank you very much for your comments on our paper! Your review and comments are very helpful to our paper, and we have learned a lot from them. We reply to your comments one by one as follows.

Comments 1: Only in the beginning, a definition of the ABL and the different layers should be helpful, e.g. Mixing Layer, Surface Inversion Layer, Capping Inversion, Convective Mixed Layer, Residual Layer.

Response: We have added the definition of the Mixing layer, surface inversion layer, capping inversion, convective mixing layer and residual layer in the latest revised paper:

“Because of the Earth's rotation, the ABL presents strong diurnal variation, leading to the formation of many different layers in the boundary layer. The mixing layer accounts for a large proportion of the ABL in the deep convective boundary layer, and at present, the height of the mixing layer is equivalent to the height of the ABL. Pollutants emitted into the ABL can reach a certain height through turbulent vertical mixing processes (Emeis and Schäfer, 2006), making it possible to determine the ABL height from the concentration of pollutants. The top of the mixing layer exhibits capping inversion. Due to a change in the surface net radiation occurring at night, a stable boundary layer begins to form at night because of the cooling effect of the ground surface, and the surface inversion layer is nearest to the ground. The nocturnal stable boundary layer is often accompanied by a residual layer that maintains the characteristics of the daytime mixing layer (Stull, 1988).” (Page2 Line7-15, revised paper).

Comments2: Usually the ABL is the turbulent layer with winds influenced by the earth surface. Within this definition the Wind Profile Radar (WPR – the full word should not only be used in the abstract) gives the best result of the ABL height. In the air quality community the mixing layer and inversion layers are more common to use in the context of air pollution concentrations. These terms are explained at the beginning of chapter 3.2. But this could be done some more concisely., perhaps extracting one day of Fig. 3 and explaining it. In Fig. 3 the heights H_c and H_u should be marked which are referred to later.

Response: We have added the full word of WPR (wind profile radar) not only in the abstract, and wind profile radar (WPR) appeared first in the introduction (Page2 line19, revised paper) and the all the abbreviations are used later in the paper. We recalculated the ABL height determined by WPR for distinct “nose” profiles. And the new ABL heights are exhibited in Fig.4 in latest revised paper. In addition, the heights H_u and H_c are marked as shown in revised paper. The definition of mixing layer and inversion layers have also been added in the revised paper. (Page2 Line7-10, revised paper)

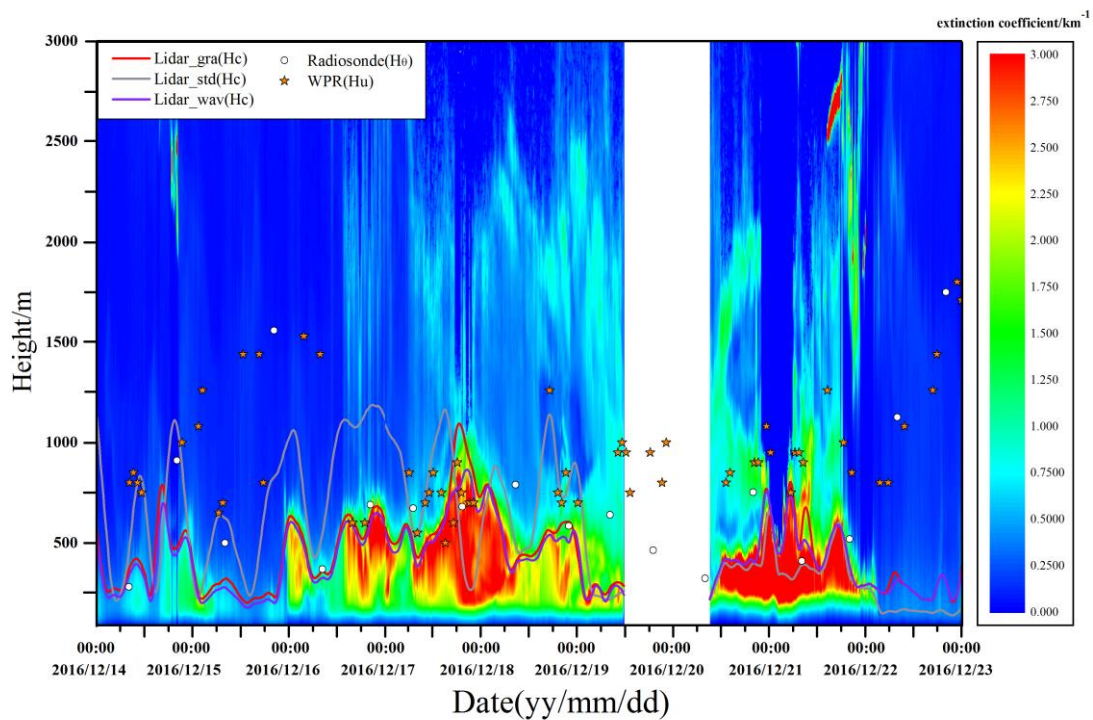


Fig.4 Temporal and spatial variations in the extinction coefficient (shaded, unit: km^{-1}) from 14 to 23 December 2016 and ABL heights (m) determined with different instruments. The red line (Lidar_gra), grey line (Lidar_std), and purple line (Lidar_wav) represent ABL heights determined by the Lidar using the gradient method, the standard deviation method, and the wavelet method, respectively. White points: ABL height determined by radiosonde; Five-pointed star: ABL height determined by WPR. It should be noted that the blank part of the extinction coefficient can be attributed to a technical failure, and lidar data for 11:00 on December 19 to 09:00 on December 20 are missing.

Comments3: Table 2: The first column shows the air quality, I think these are PM_{2.5} concentration ranges. It should be mentioned. There is a general influence of humidity. But not so clear. That is why the humidity depends on the origin of the advected air (more wet or more dry). Important is the decrease jump at the inversion layer, shown in Fig. 4 and not the absolute value of the humidity. Page 13 line 5... "Hc is even heightened slightly but Hu (not Hc) reduces by..."

Response: For table2, we have explained the PM_{2.5} concentration of the corresponding air quality in the table1 head, and we also accept the idea of reviewer to reexplain it in the table2 header (Page19, Table2, revised paper). As for page13 line5, "Hc is even heightened slightly but Hu (not Hc) reduces by..." thank you very much for your carefulness and we have corrected this error (Page20, Line12, in the revised paper).

Comments4: In the conclusion the role of the mixing layer and the inversion layers should be highlighted in the context with air pollution concentrations. And these layers are best determined by radiosonde soundings and lidar. The tower measurements are also helpful to determine the surface inversions height, if the inversion layer is lower than the tower height. With the Wind Profile Radar (WPR) the height of the Atmospheric Boundary Layer (turbulent) can be well determined. But for the air pollutant concentrations (PM 2.5) the inversion Layers and the Mixing Layer are relevant which is shown in this paper.

Response: In revised paper, we have highlighted the relationship between mixing layer, inversion layer and pollutant concentration in the conclusion.

“The inversion layer is closely related to the concentration of pollutants. Pollutants emitted in the ABL generally accumulate under the inversion layer. The inversion layer’s height decreased significantly during the pollution period, and the lowest value was measured at below 500m.” (Page20, Line8-10, revised paper).

4. Response to the Editorial corrections

a) The manuscript needs heavy editorial corrections throughout.

Response: We have carefully revised and edited the full text of the paper and many details have been rewritten.

b) P. 3, line 12: 49 m above sea level is listed twice in this sentence. Remove one instance.

Response: One of the two “49m” was removed. (Page4 line1, in the revised paper)

b) P. 3, line 13: Why is ‘August 1979’ here?

Response: P.3 line 13: Our original intention is that this tower was established in 1979 and has been revised in paper.

Multiple technical observations of the atmospheric boundary layer structure of a red warning haze episode in Beijing

Yu Shi^{1,2}, Fei Hu^{1,2}, Guangqiang Fan³, and Zhe Zhang^{1,2}

¹State Key Laboratory of Atmospheric Boundary Layer Physics and Atmospheric Chemistry, Institute of Atmospheric Physics, Chinese Academy of Sciences, Beijing 100029

²University of Chinese Academy of Sciences, Beijing 100049

³Key Laboratory of Environmental Optics and Technology, Anhui Institute of Optics and Fine Mechanics, Chinese Academy of Sciences, Hefei 230031

Correspondence: F.Hu (hufei@mail.iap.ac.cn)

Abstract. The study and control of air pollution ~~need-to-detect~~ involves measuring the structure of the atmospheric boundary layer (ABL) to understand the mechanisms of the interactions occurring between the atmospheric boundary layer and air pollution. However, when extreme pollution occurs, the detection of atmospheric boundary layer structures is very limited. Beijing, the capital of China, experienced severe levels of haze pollution in December 2016, and the city issued its first red
5 air pollution warning of the year (the highest $PM_{2.5}$ concentrations were later found to exceed $450\mu g m^{-3}$). In this paper, the vertical profiles of wind, temperature, humidity and the extinction coefficient (reflecting aerosol concentrations) as well as ABL heights and turbulence quantities under heavy haze pollution conditions are analyzed, with data collected from Lidar,
wind profile radar (WPR), radiosonde, a 325-meter meteorological tower (equipped with a 7-layer ultrasonic anemometer and 15-layer low frequency wind, temperature and humidity sensors) and ground observations. The ABL heights obtained
10 by three different methods based on Lidar extinction coefficient data (H_c) are compared with the heights calculated from radiosonde temperature data (H_θ) and from WPR wind speed data (H_u). The results show that increases in water vapor have greatly promoted the hygroscopic growth of aerosols and that corresponding extinction coefficient levels have also increased significantly. The ABL heights of H_θ and H_u ~~of heavy~~ measured on days with heavy levels of haze pollution were generally lower than those measured on days without pollution, but the H_c levels increased. Turbulence and pollutant concentrations are
15 closely related during periods of haze pollution, and time changes in friction velocity (u_*) and turbulent kinetic energy (TKE) are clearly inversely correlated with $PM_{2.5}$ levels. The results ~~of this paper could provide some~~ in this paper can serve as a reference for the parameterization of boundary layer heights and turbulent diffusion ~~process-in~~ processes for the numerical model of severe air pollution.

1 Introduction

20 Air pollution has an important impact on human health, weather, climatic patterns and the ecological environment (Seinfeld and Pandis, 1997; Brook et al., 2004; Ding et al., 2013; Wang et al., 2014a; Zhang et al., 2015a). The pollutants emitted as a result of human activities are mainly confined to the atmospheric boundary layer (ABL), which is the lowest part of the troposphere and

about is approximately 1~2 km from the ground. In particular, fog and haze, which have a strong influence on visibility and air quality levels, mainly occur in the ABL (Cao et al., 2004; Chan and Yao, 2008; Fu et al., 2008; Liu et al., 2012). Because the formation, evolution, and diffusion of air pollutants are closely related to ABL structures and turbulence characteristics (Zhang et al., 2011; Wei et al., 2018), research on the ABL is important for understanding air pollution mechanisms and for developing pollution control strategies. On the other hand, the relationships between the ABL and atmospheric pollution are very complex and involve multiscale nonlinear physical and chemical processes; thus, both theoretical research and numerical simulations have encountered difficulties (Sun et al., 2013; Huang et al., 2014; Wang et al., 2014b; Miao et al., 2018). Therefore, it is very necessary to obtain first-hand information from observation experiments. Because of the Earth's rotation, the ABL presents strong diurnal variation, leading to the formation of many different layers in the boundary layer. The mixing layer accounts for a large proportion of the ABL in the deep convective boundary layer, and at present, the height of the mixing layer is equivalent to the height of the ABL. Pollutants emitted into the ABL can reach a certain height through turbulent vertical mixing processes (Emeis and Schäfer, 2006), making it possible to determine the ABL height from the concentration of pollutants. The top of the mixing layer exhibits capping inversion. Due to a change in the surface net radiation occurring at night, a stable boundary layer begins to form at night because of the cooling effect of the ground surface, and the surface inversion layer is nearest to the ground. The nocturnal stable boundary layer is often accompanied by a residual layer that maintains the characteristics of the daytime mixing layer (Stull, 1988). The ABL height is closely related to air pollution, but it is not the only factor that shapes air quality. Pollution conditions are also affected by wind speeds, emissions, chemical processing, etc. (Schäfer et al., 2006; Geiß et al., 2017). Some works have compared ABL heights based on lidar and radiosonde data, and the correlations between them are stronger under unstable conditions (Emeis and Schäfer, 2006; Martucci et al., 2006). However, for ABL heights determined from wind profiler radar (WPR), relatively fewer studies have compared and analyzed the results of lidar and radiosonde tests applied during haze pollution episodes.

Regarding air pollution, many observational experiments have been conducted internationally, especially with reference to air pollution in the ABL over urban areas (i.e., the urban boundary layer). Examples of such projects include European Cooperation in the Field of Scientific and Technical Research, abbreviated as COST715 (Fisher et al., 2001); URBAN 2000, a major urban tracer and meteorological field campaign conducted in Salt Lake City, Utah, in October 2000 (Allwine et al., 2002); Joint Urban 2003, a field experiment conducted in October 2003 in Oklahoma City (Wang et al., 2007); MIRAGE 2006, Megacity Impacts on Regional and Global Environments (Lance et al., 2012); and SURF, the Study of Urban impacts on Rainfall and Fog/haze (Liang et al., 2018).

A meteorological tower serves as one of the best platforms from which to detect the ABL structure under conditions of atmospheric pollution (Quan and Hu, 2009; Sun et al., 2015; Ren et al., 2018). Although the height of such a tower is limited, the boundary layer is basically stable when heavy pollution occurs, and the ABL height is low, so it is easy to measure from a tower. Conventional meteorological and turbulence instruments installed at different heights above a meteorological tower can obtain information on stable boundary layer structures and turbulence diffusion parameters (Katul et al., 1995). Traditional detection methods include tethered balloon, radiosonde, WPR tools, which can detect higher heights (Grimsdell and Angevine, 1998; Andreas et al., 2000; Kalapureddy et al., 2007; Li et al., 2015; Han et al., 2018). In recent decades, aerosol laser

radar (Lidar) has been used increasingly extensively. It can be used to retrieve the vertical distribution of particles from Lidar backscattering data (Wang et al., 2012; Summa et al., 2013; Jiannong et al., 2013; Bravo-Aranda et al., 2017). It is impossible to obtain information on the boundary layer structure and on the interrelationships between pollutants found in atmospheric pollution (especially in heavy haze) unilaterally by means of the above-mentioned technical techniques, and it is necessary to carry out comprehensive observations simultaneously.

From 14 to 22 December 2016, Beijing, the capital of China, experienced a period of severe haze pollution. The government issued its highest air pollution warning (red alert) during this period. Beijing is a densely populated city covering an area of approximately 396 square kilometers (see Fig.1b). Despite strong pollution control measures taken by the government, the average $PM_{2.5}$ concentration per hour rose from $20\mu g m^{-3}$ to more than $450\mu g m^{-3}$ (see Table.1) in just five days. What are the mechanisms of episodes of such severe air pollution? Addressing this question requires conducting a comprehensive and in-depth analysis of weather conditions, pollutant emissions, regional transport processes and physicochemical transformation mechanisms and of interactions between haze and boundary layer structures (Huang et al., 2014; Sun et al., 2014; Ding et al., 2016). Some previous studies have been conducted on haze events in the Beijing area (Li et al., 2017; Sheng et al., 2018; Wang et al., 2018), especially physical and chemical mechanism analyses based on comprehensive observation data from tall towers (Sun et al., 2006; Guo et al., 2016).

The purpose of this paper is to investigate the ABL's structure and turbulence characteristics measured during the red haze warning period of 2016 by means of tower, Lidar, WPR and radiosonde approaches. The paper includes a brief introduction of weather patterns, of heavy haze pollution trends and of our observation sites and techniques; an analysis of boundary layer winds, temperatures, humidity profiles, and extinction coefficients (reflecting the concentration of haze particles); and ABL heights determined by different detection techniques. The vertical distributions of turbulent quantities are also outlined. Finally, avenues for further research are given.

2 Observation sites, instruments and data

The ABL observation data of this paper are mainly obtained in used for this paper mainly cover three locations in Beijing. The first area is located at the Institute of Atmospheric Physics (IAP) of the Chinese Academy of Sciences, where there are a 325 meter high meteorological tower and a Lidar. The second is positioned approximately 600 meters away from the east side of this tower where a wind profile radar (WPR) system is based. The third area is the observatory of the Beijing Meteorological Bureau, which is approximately 20 kilometers away from the tower. Conventional ground meteorological observations and radiosonde data from the WMO station are used (ZBAA in Fig.1b). The above observation sites are shown in Figure 1b. The topography around Beijing is also given in Figure 1a. The time used in this paper is the We use local station time in this work, and the observational instruments and data employed are as follows:

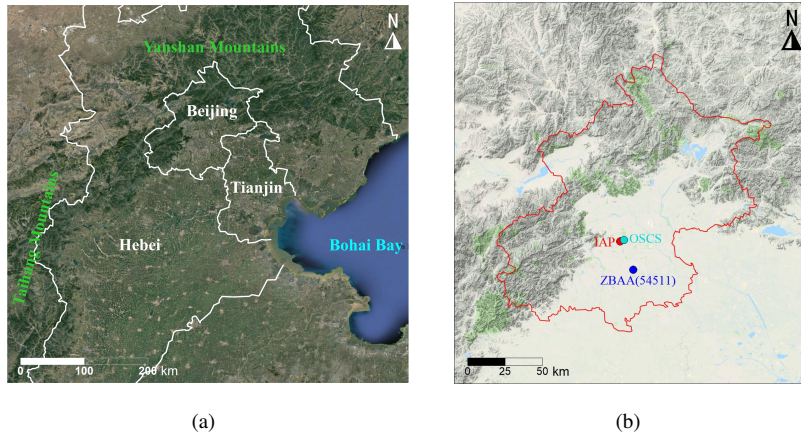


Figure 1. Local topography of Beijing and of its surrounding area (a). The locations of observation sites in Beijing (b): red circle: IAP (Lidar), blue circle: ZBAA radiosonde observation station, cyan circle: pollution observation station (OSCS) positioned approximately 2 km northeast of the Lidar. Beijing is a densely populated city covering an area of approximately 396 square kilometers.

- 1) The IAP's meteorological tower is positioned 49 meters above sea level, is 325 meters tall, and is located at (39°58'N, 116°22'E, ~~49m above the sea level~~) between the Beijing North Third Ring Road and North Fourth Ring Road ~~from August 1979~~. A total of 15 observation platforms (at 8, 15, 32, 47, 65, 80, 103, 120, 140, 160, 180, 200, 240, 280 and 320 m) are set up on the tower, and wind speed (MetOne, USA), wind direction (MetOne, USA), temperature (HC2-S3, Switzerland) and humidity (HC2-S3, Switzerland) observation instruments are mounted onto each platform. In addition, 7 sets of three-dimensional ultrasonic anemometers (Wind Master, Gill, USA) and water vapor / carbon dioxide analyzers (LI-7500, USA) are installed on the tower (at 8, 15, 47, 80, 140, 200 and 280 m). All turbulence data sampling ~~frequency is~~ frequencies are set to 10 Hz. All of the tower data are averaged for 20 minutes. A detailed description of the meteorological tower can be found in (Al-Jiboori and Fei, 2005) and (Chen et al., 2018) and on the website (<http://view.iap.ac.cn:8080/imageview/>).
- 2) The extinction coefficients were measured by a Lidar system (AGHJ-I-Lidar, China) installed underneath the 325 m tower. The Lidar can provide backscattering signals at wavelengths of 532 nm and 355 nm at a vertical resolution of 7.5 m and a temporal resolution of approximately 5~10 min. Due to technical failures, lidar data are missing for 11:00 on December 19 to 09:00 on December 20, 2016;
- 3) Wind speeds and wind directions were also monitored by means of WPR (Airda3000, China) during red-alert pollution periods. In this paper, the temporal resolution of WPR is set to 5 min, and the vertical resolution is set to 50 m below 1000 m and 90 m above 1000 m.
- 4) ~~High-resolution vertical profile radiosonde data collected~~ twice daily (08:00 and 20:00 Beijing time) were retrieved from the University of Wyoming's website (<http://weather.uwyo.edu/>) for Beijing's meteorological observatory station, which is named ZBAA in international code (Fig.1b). Surface visibility and other normal meteorological variables were routinely measured with a temporal resolution of half an hour in ZBAA.

5) Surface measurements of six kinds of air pollutants ($PM_{2.5}$, PM_{10} , NO_2 , SO_2 , CO and O_3) with a temporal resolution of one hour can be found on the official website of the Beijing Environmental Protection Agency (<http://beijingair.sinaapp.com/>). The data used in this paper **comes were collected** from the environmental monitoring station (Olympic Sports Center Station) positioned closest to the tower (approximately 2 km northeast).

5 3 Results and discussion

3.1 Surface observations of haze and meteorological conditions

From 14 to 22 December 2016, complete haze pollution was observed in the Beijing area (see Table 1). The generation, accumulation and elimination of $PM_{2.5}$ were recorded. We can see that from 20 to 21 December, the hourly average $PM_{2.5}$ concentration was almost maintained at approximately $400 \mu g m^{-3}$ over 48 hours, which greatly exceeded the air pollution limits (i.e., $250 \mu g m^{-3}$) set by China's State Environmental Protection Administration. Figure 2 shows the concentration time series for $PM_{2.5}$, wind speed and direction, temperature, relative humidity (RH), surface pressure and visibility for this period of heavy haze pollution .

Table 1. Daily average data for six major air pollutants in Beijing measured during a period of heavy pollution from 14 to 23 December 2016: $PM_{2.5}$, PM_{10} , NO_2 , SO_2 and O_3 (units are $\mu g m^{-3}$); CO ($mg m^{-3}$). Data sources: <http://beijingair.sinaapp.com/>; according to the "Technical Specification for Air Quality Index(HJ 633-2012)" issued by China's National Environmental Protection Agency, based on $PM_{2.5}$ concentrations air pollution levels can be divided into five levels, i.e., good($0\sim 75 \mu g m^{-3}$), slightly polluted ($75\sim 115 \mu g m^{-3}$), moderately polluted ($115\sim 150 \mu g m^{-3}$), heavily polluted ($150\sim 250 \mu g m^{-3}$), and seriously polluted ($>250 \mu g m^{-3}$).

Date	Air Quality	AQI index	$PM_{2.5}$	PM_{10}	NO_2	SO_2	CO	O_3
2016-12-14	Good	60	24	38	42	9	0.74	32
2016-12-15	Good	83	25	51	40	9	0.85	31
2016-12-16	Slightly Polluted	274	101	134	87	20	2.07	8
2016-12-17	Heavily Polluted	351	184	211	102	30	3.14	5
2016-12-18	Seriously Polluted	337	219	245	100	24	3.42	7
2016-12-19	Seriously Polluted	306	214	247	107	22	3.88	7
2016-12-20	Seriously Polluted	342	365	422	133	8	7.67	4
2016-12-21	Seriously Polluted	363	393	429	152	10	7.97	4
2016-12-22	Moderately Polluted	325	93	170	45	6	1.95	39
2016-12-23	Good	55	31	42	43	7	0.74	26

Generally, visibility serves as a representative index of air quality and atmospheric diffusion capacity (Zhang et al., 2015b). Figure 2 shows that when the concentration of $PM_{2.5}$ increased to high levels, visibility quickly deteriorated. Visibility on clean days was largely measured as greater than 10 km, and when the $PM_{2.5}$ concentrations reached approximately 200~300

$\mu\text{g m}^{-3}$, the visibility decreased to 2~5 km. Even when $\text{PM}_{2.5}$ reached approximately $400 \mu\text{g m}^{-3}$, visibility dropped sharply to 1 km or to hundreds of meters. The surface pressure results suggest that air pressure levels decreased from approximately 1035 hPa to 1023 hPa, and in general, Beijing was controlled by a weak high-pressure system during the pollution episode. The RH taken from ground observations shows significant diurnal variations and an obvious anti-correlation between RH and temperature. From 20 to 21 December, the diurnal variation in temperature and relative humidity in heavy pollution was greatly suppressed, and a further analysis of MODIS images (see Fig. 3) during this period shows that the pollution process was indeed accompanied by fog, while pollution formed in the south-central area of Hebei Province on 15 December 2016 and then spread across the whole Beijing-Tianjin-Hebei area on 18 December. Stratiform clouds appeared in areas surrounding Beijing on 21 December, but due to the high concentrations of pollutants ($\text{PM}_{2.5}$ values approaching $400 \mu\text{g m}^{-3}$), mixed fog and haze appeared in Beijing. During the day, pollutants can scatter more solar radiation while the ground receives less solar radiation, leading to the suppression of diurnal variations in temperature and relative humidity on the ground (Gao et al., 2015). An increase in RH occurs due to a decrease in temperature but is also the result of a surge in water vapor. For example, in the early morning, temperature differences observed between 17 and 20 December were minor, and the RH on 17 December was approximately 80%, while the RH in the early morning of 20 December reached nearly 100%, indicating an increase in water vapor levels in the Beijing area at this time. The surface wind speed during the pollution episode fell to almost less than 2 m s^{-1} and can be basically regarded as a stagnant weather system dominating ABL processes and resulting in poor air quality. From Fig. 2, we can see that there were cold fronts (strong NW winds) on both 15 December and 22 December, which advected pollutants away, resulting in good air quality. Between the fronts, $\text{PM}_{2.5}$ levels slowly increased, as the air was stagnant (weak and variable winds in between), and the pollutants that were emitted locally slowly built up. The wind direction also seemed to be cyclical on each day in response to local mountain valley circulation around Beijing (Hu et al., 2005). According to other studies, stronger northerly winds occurring in the winter are the main mechanisms through which pollution is removed, leading to good air quality (Sheng et al., 2018).

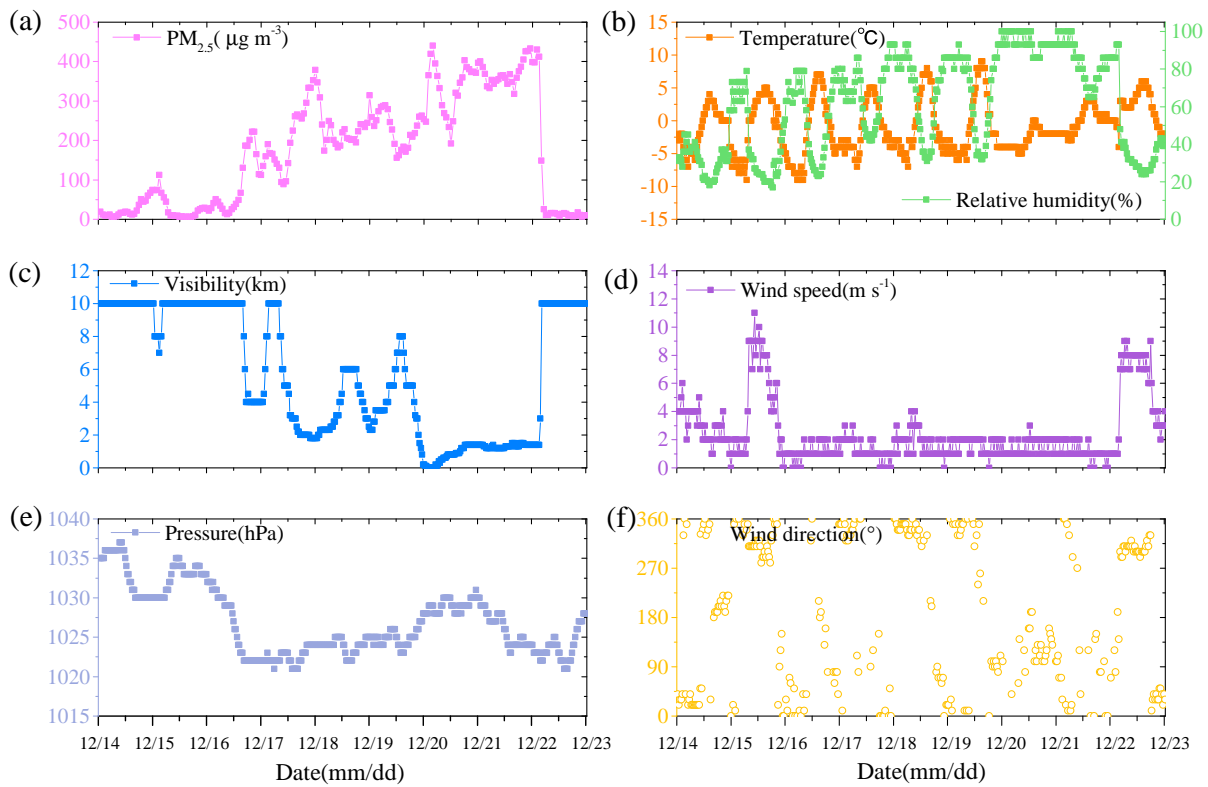


Figure 2. Time series of ground level PM_{2.5} (a), relative humidity and temperature (b), visibility (c), wind speed (d), surface pressure (e) and wind direction (f) during 14 to 22 December 2016; the units for these meteorological parameters are as follows: $\mu\text{g m}^{-3}$, %, °C, km, m s^{-1} , hPa and ° respectively.

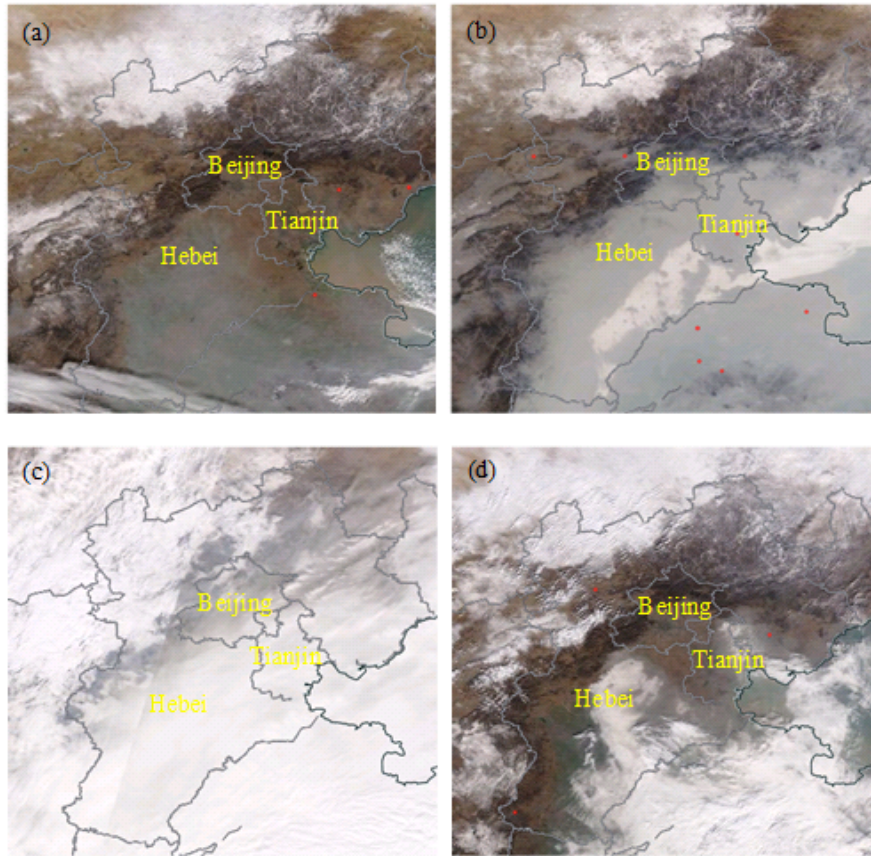


Figure 3. MODIS images of the Beijing-Tianjin-Hebei region on 15 December (a), 18 December (b), 21 December (c), and 22 December (d).

3.2 Boundary layer heights observed by Lidar

The most basic definition of the ABL height is the height at which the influence of the Earth's surface on the lower troposphere disappears. This influence applies not only to conventional meteorological elements but also to turbulence quantities and even more for substances in the atmosphere such as aerosols, water vapor and nonreactive tracer gases (Seibert et al., 2000). Levels of various pollutants and water vapor in the ABL are much higher than those found in the free atmosphere, and therefore, there is often an obvious aerosol concentration gradient between the boundary layer and the free atmosphere. The extinction coefficient reflects the degree of aerosol particle scattering from lasers in the atmosphere (Boers and Eloranta, 1986). Thus, the ABL height can also be estimated from the extinction coefficient gradient. We used three popular methods—the gradient method (Lidar_gra) (Flamant et al., 1997), the standard deviation method (Lidar_std) (Hooper and Eloranta, 1986) and the wavelet method (Lidar_wav) (Cohn and Angevine, 2000; Davis et al., 2000; Brooks, 2003)—to extract boundary layer heights from extinction coefficients (continuous Haar wavelet transformation was used in this paper, taking dilation paramet $a=6$).

The ABL height determined by Lidar is represented by H_c . In this study, the Lidar_gra method applies the height of the atmosphere at which the gradient of the Lidar extinction coefficient reaches its most negative value. The standard deviation of the extinction coefficient reflects the degree of Lidar echo signal dispersion at different heights. The top of the planetary boundary layer constitutes the intersection between air in the boundary layer and the free atmosphere, which leads to a strong signal change at the top of the boundary layer. We define the height of the maximum standard deviation of signals as the ABL height. The Lidar_wav method can also be used to detect abrupt changes in signals, so we use the Haar wavelet and take the height at which the wavelet coefficient is at its highest value as the height of the ABL. These methods are used to find the abrupt change in the extinction coefficient occurring at the top of boundary layer, though they present their own limitations.

Generally, the atmospheric boundary layer can be divided into a daytime convective mixing layer and a nighttime stable boundary layer. In the morning, the well-mixed convective boundary layer (CBL) is growing and often reaches its maximum height in the early afternoon. In the afternoon, the CBL gradually transforms into a neutral boundary layer. Figure 4 illustrates the evolution of ABL heights measured with Lidar, WPR and radiosonde tools.

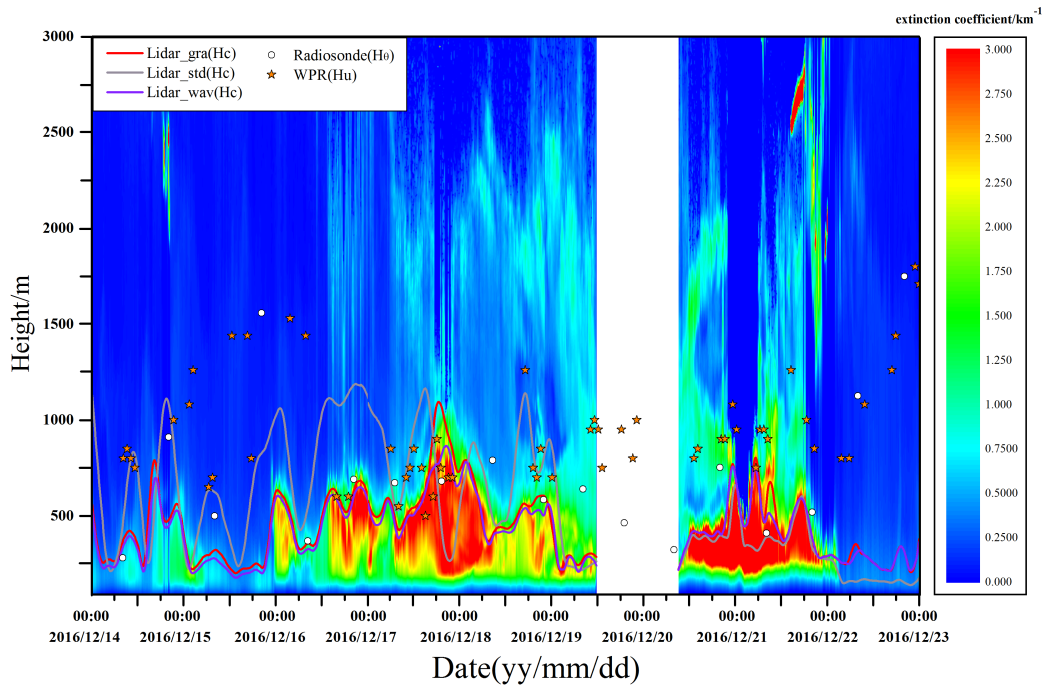


Figure 4. Temporal and spatial variations in the extinction coefficient (shaded, unit: km^{-1}) from 14 to 23 December 2016 and ABL heights (m) determined with different instruments. The red line (Lidar_gra), grey line (Lidar_std), and purple line (Lidar_wav) represent ABL heights determined by the Lidar using the gradient method, the standard deviation method, and the wavelet method, respectively. White points: ABL height determined by radiosonde; Five-pointed star: ABL height determined by WPR. It should be noted that the blank part of the extinction coefficient can be attributed to a technical failure, and lidar data for 11:00 on December 19 to 09:00 on December 20 are missing.

The determination of the ABL height by means of the Lidar method is based on the vertical profiles of the extinction coefficient or the aerosol concentration. When concentrations of $\text{PM}_{2.5}$ are high, the weakening effects of aerosol particles on lasers are stronger. ABL heights determined by Lidar_gra and Lidar_wav were almost the same, with a correlation coefficient of nearly 95%. From 16 to 18 December and from 20 to 21 December, the ABL heights were approximately 500~750 m. Furthermore, the ABL height determined by the Lidar_std method was slightly higher than that derived from both methods. During a period of heavy pollution (20 to 21 December), the extinction coefficient quickly exceeded 3 km^{-1} at 250 m aboveground. Perhaps due to the accumulation of pollutants, H_c did not seem to decline on these days. When the atmosphere was relatively free of pollutants, such as on 15 or 22 December, the aerosol concentration was low and the extinction coefficient derived from the Lidar system displayed no obvious signs of decline from the ground to the upper height. The ABL heights obtained by these methods based on the Lidar system are clearly lower than those obtained by the other instruments. If we were to continue

to use the Lidar system to determine the height of the boundary layer, it would have been distorted. Therefore, the continuous observation of the ABL height can be achieved by means of other instruments or improved methods based on the Lidar system.

3.3 Boundary layer structure observed by radiosonde technologies

Radiosonde ~~is instruments are~~ the most widely used tools for conventional meteorological observation ~~method in the world~~.

5 The white points shown in figure 4 denote the ABL height determined from radiosonde data. The potential temperature (θ) determined by radiosonde technology is calculated from the following formula: $\theta=T+\gamma_d z$. $\gamma_d=0.00975 \text{ K m}^{-1}$, and T is the measured temperature. As noted in many previous studies, the most widely used approach for the determination of the ABL height and structure for the daytime and nighttime involves identifying local maxima in potential temperature vertical gradient profiles as measured by radiosonde devices (Seibert et al., 2000; Summa et al., 2013; Sorbjan, 1989), but this method is only
10 appropriate to apply to the convective ABL (Hennemuth and Lammert, 2006). Since the pollution period we examine involves stagnant winter weather conditions and as our radiosonde data only apply to dawn and dusk periods (08:00 h and 20:00 h), a stable boundary layer often appears (see Fig. 5, for example), and the height of the stable boundary layer (SBL) is more difficult to determine (Keller et al., 2010; Jong et al., 2015; Schäfer et al., 2006). **In this study, the level showing an obvious change in the potential temperature gradient and the profile of relative humidity were used to define the ABL height, as expressed by**
15 **H_θ** (see the blue dotted lines in Fig. 5). Under stagnant and heavily polluted weather conditions, turbulence is more heavily suppressed than under normal weather conditions, and the top of the residual layer can also characterize the thickness of the stable boundary layer to some extent. We can also use the minimum value of the relative humidity (green curves shown in Fig. 5) gradient to determine the height of the SBL. The atmospheric stratification of potential temperatures and RH can affect the distribution of aerosol concentrations, which in turn affects the extinction coefficient. In Fig. 5, vertical profiles of the
20 extinction coefficient observed by Lidar during the same period are also given.

As shown in Fig. 5, the pollution episode was often accompanied by an inversion layer, as the vertical gradient of PT is positive, implying that the atmosphere was basically stable. The fact that the PBL was stable is unsurprising given the timing of radiosonde profiles for 08:00 and 20:00 local time, which respectively occur approximately 30 min after sunrise and 3 hours after sunset during the experimental period. Thus, a nocturnal inversion should barely be eroded by 08:00 (if at all, depending
25 on the energy balance as insolation levels are low), and a nocturnal inversion should form by 20:00. Due to this timing, these profiles are not representative of daytime conditions when pollutants are actively mixed. Midday profiles (noon local time or the early afternoon) would instead present instability and mixing. Air pollutants are generally blocked below the inversion layer and are not easily diffused to high levels. Figure 5a shows that H_θ at 20:00 on 16 December was approximately 690 m, where the potential temperature was approximately 280 K and the RH was approximately 20%, and the extinction coefficient was
30 also reduced to 0.7 km^{-1} . **Due to the cooling effects of surface longwave radiation, the ground inversion layer formed from the surface at a depth of approximately 100 m. At this time, the potential temperature gradient underwent an obvious change at 600 m. The inversion intensity levels below 600 m was weaker, and the height H_θ was approximately 690 m.** The most negative value of the extinction coefficient gradient appeared at approximately 500 m at this time, and the extinction coefficient below 690 m was much higher than that observed above 690 m, indicating that aerosol particles were mainly concentrated below the

inversion layer (Baumbach and Vogt, 2003) and that the H_θ calculated by radiosonde is basically consistent with H_c determined by Lidar.

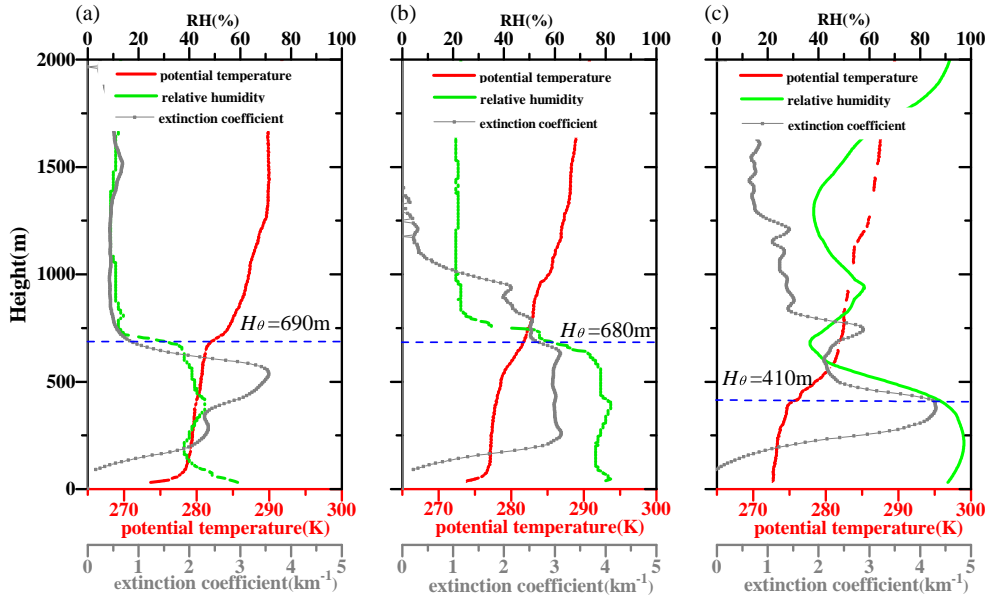


Figure 5. Vertical profiles measured from the ZBAA meteorological station. (a) 20:00, 16 December 2016 (b) 20:00, 17 December 2016 (c) 08:00 21 December 2016. Red line: potential temperature (K); Green line: RH (%); Grey line: extinction coefficient (km^{-1}); Blue dotted line: ABL height determined by radiosonde and expressed in H_θ (m).

At 20:00 on 17 December, ground inversion started to form. H_θ was observed at approximately 680 m, and the potential temperature at this level was still at approximately 280 K, though the RH reached nearly 60%. Below this height, the whole atmosphere layer had developed a high humidity layer with an RH of nearly 80% from the ground, and the corresponding extinction coefficient had also increased significantly. The extinction coefficient between 250~600 m was almost 3 km^{-1} , revealing that the concentration of aerosols had increased significantly. Combined with the wind direction at this time (Fig.7d), it is clearly observed that the transport of easterly winds moved considerable levels of water vapor from Bohai Bay (approximately 200 kilometers east of Beijing), which promoted the hygroscopic growth of aerosol particles (Svenningsson et al., 1992; Chuang, 2003; Pan et al., 2009). At 08:00 on 21 December, the potential temperature distribution in the morning was different from that observed at 20:00, and the surface temperature had begun to increase as solar radiation was received and the H_θ was approximately 410 m. ~~The ground inversion layer has disappeared and the H_θ was about 604 m.~~ The value below 300 m was nearly 95%, while the maximum extinction coefficient, which exhibited bimodal features, reached nearly 4 km^{-1} . The altitude at which the extinction coefficient reached peak levels in the lower layer was approximately H_θ . By means of analyzing and comparing H_c and H_θ values it is apparent that when concentrations of $\text{PM}_{2.5}$ were high, the accumulation of pollutants was mainly accompanied by the inversion layer in the atmosphere. ~~The potential temperature gradient at the inversion layer is generally larger.~~ Even though H_c reflects aerosol scattering information and H_θ denotes potential temperature characteristics,

there is a strong correlation between them with a correlation coefficient of approximately 72%. ~~However, when the atmosphere was clean, the aerosol concentration was obviously reduced and the inversion layer was not so significant.~~ As shown in Fig.4, H_θ was significantly higher than H_c determined by the three methods based on the Lidar extinction coefficient.

3.4 Boundary layer structure observed by WPR

- 5 The ground is the most important sink of atmospheric momentum, and the wind speed is zero at the Earth's surface. The ABL wind speed ~~changes gradually from the~~ gradually changes from the Earth's surface to the geostrophic winds measured at high altitudes, and the wind information extracted from the WPR has been widely used to determine the ABL height (Cohn and Angevine, 2000; Bianco and Wilczak, 2002). A comprehensive review of estimated convective boundary layer heights is given by Seibert et al (2000). Because our WPR wind speed observations ~~have~~ reveal the presence of many low-level jets or maxima,
- 10 we used the height of the low level maximum wind speed as the ABL height (Banta, 2008; Pichugina and Banta, 2010; Devara et al., 1995), expressed in H_u . Figure 6 shows wind speed profiles observed by WPR on December 15, 17, 19 and 21, from which we find that wind extremes and weak low-level jets often occur at below 1000 meters.

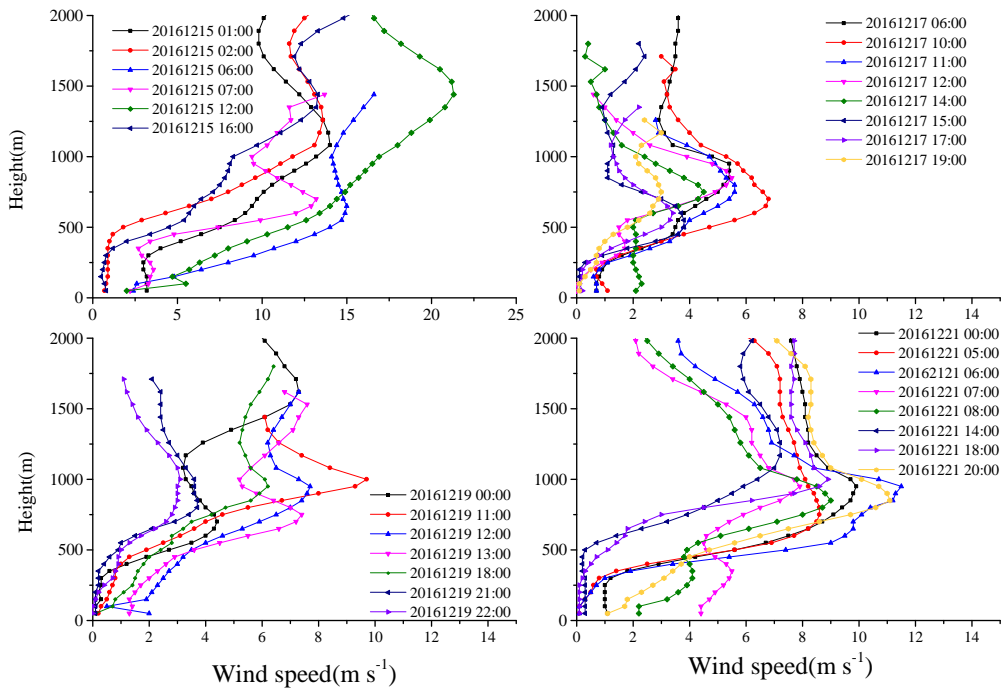


Figure 6. Vertical wind profiles measured by WPR on December 15, 17, 19 and 21, 2016. December 21 is the most polluted day when there are obvious low-level jets.

As shown in Fig. 4, H_u was much higher than H_c , especially on the unpolluted day when the H_u was approximately 1500 m. With an increase in $PM_{2.5}$ concentrations, H_u also decreased; that is, the height of the low-level maximum wind velocity should also decrease when the atmosphere is polluted. In this case, H_u , H_c and H_θ were very close. To analyze the influence of the boundary layer's wind structure on pollutants, we further discuss the representative wind speed and direction profiles of the three typical days for the unpolluted and polluted conditions. As is shown in Fig. 7, wind speeds below 1000 m did not exceed 6 m s^{-1} on 17 December, and the H_u determined by WPR ranged from 750~1000 m. At 12:00 a typical "nose" profile distribution formed according to the wind profile with a maximum value observed in the middle of the wind profile. The wind direction profiles show that the wind direction from the ground to approximately 750 m was northeast ($0^\circ \sim 90^\circ$), and the wind direction observed above 750 m was northwest ($270^\circ \sim 360^\circ$). Furthermore, the wind directions from 750~2000 m remained basically stable in the northwest direction, echoing geostrophic winds. At this time, the height of the maximum wind speed fit well to the height of the wind direction and geostrophic wind began to form. In addition to 12:00 on 17 December, at other four times almost strictly north-eastern winds formed below 1000 m, and winds began to transform into the northwest winds at different heights. Wind speeds increased to some extent on 21 December with typical "nose"-type wind speed distributions observed at 00:00, 08:00 and 20:00. From the ground to 2500 m steady southwest winds formed at 00:00, and the maximum wind speed was approximately 900 m. At this time, the extinction coefficient was also very low above 750 m (shown in Fig. 6), demonstrating that pollutants also formed below a height of H_u . At 12:00 the wind speed began to decrease slightly from the ground, and no obvious changes were observed beyond approximately 1100 m where wind speeds reached approximately 4 m s^{-1} . Except at 00:00 on 21 December when southwest winds prevailed from the ground to high altitudes, the wind directions shifted to the northwest at other times though these wind speeds were less strong below 500 m, and wind speed maximum values formed at a height of approximately 1000 m.

~~The wind directions of the~~ Wind directions observed on 22 December were northwest from the low layer to the high layer, but the distribution of wind velocity profiles differed from that of 21 December. Wind speeds were based on no significant maximum value area, and the maximum wind speed of 500 m approached close to 12 m s^{-1} . According to the extinction coefficient distribution (shown in Fig.4), the $PM_{2.5}$ concentration was greatly reduced on this day. H_u determined by WPR and H_θ obtained by radiosonde were relatively similar at this time, and both were far higher than H_c .

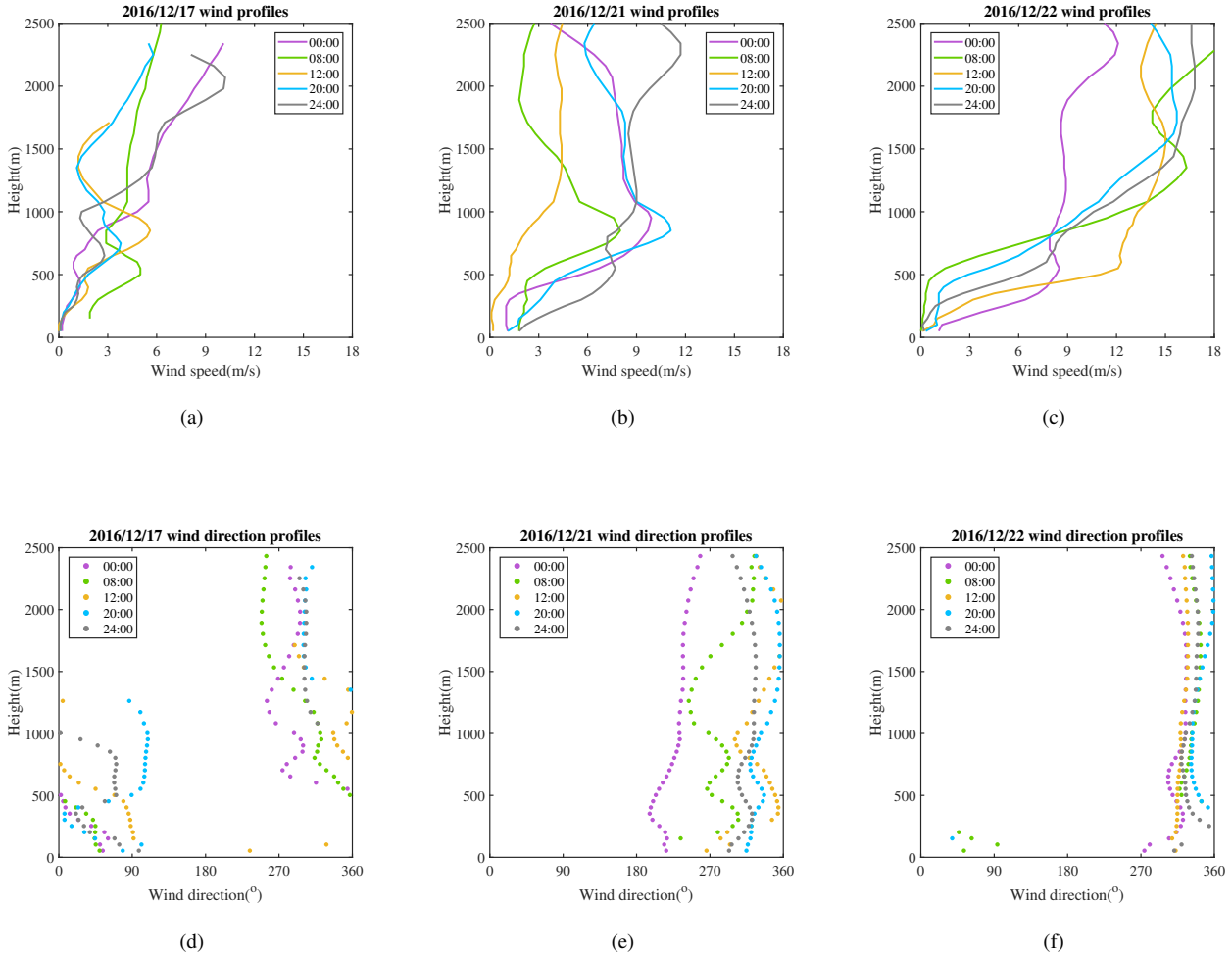


Figure 7. Vertical profiles of wind speed (m s^{-1}) and wind direction ($^{\circ}$) observed by WPR. (a) and (d): 16 December, 2016; (b) and (e): 21 December, 2016; (c) and (f): 22 December, 2016.

3.5 Boundary structure and turbulence quantities observed from the 325 m tower

Based on high-resolution gradient observations (15-layer mean and 7-layer turbulence measurements), we can analyze the relationship between $\text{PM}_{2.5}$ and low-level turbulence, average wind speed and temperature. As shown in Fig. 8, both turbulent kinetic energy (TKE) and friction velocity (u_*) at 140 m and 280 m were inversely correlated with ground level $\text{PM}_{2.5}$ concentrations. TKE and u_* can be calculated as follows (Stull, 1988): $TKE = \frac{1}{2}(\overline{u'^2} + \overline{v'^2} + \overline{w'^2})$; $u_* = (\overline{u'w'^2} + \overline{v'w'^2})^{1/4}$. The maximum TKE levels observed on unpolluted days (15 to 16 December) reached approximately $7 \text{ m}^2 \text{ s}^{-2}$ at 140 m while the TKE levels measured on hazy days (17 to 21 December) decreased sharply to very low values. After the start of the period of heavy haze pollution, TKE levels remained relatively low, and the change in TKE was not as significant when concentrations of $\text{PM}_{2.5}$ increased from $200 \sim 400 \mu\text{g m}^{-3}$. On the other hand, the time series for u_* is slightly different from that of TKE. It

seems that the inverse correlation between u_* and $PM_{2.5}$ is more obvious than that of TKE for the heavy pollution period. In fact, even during the period of heavy haze, a slight fluctuation (diurnal variation) in $PM_{2.5}$ concentrations can be observed, and the diurnal variation in u_* follows the opposite pattern to that of the $PM_{2.5}$ phase.

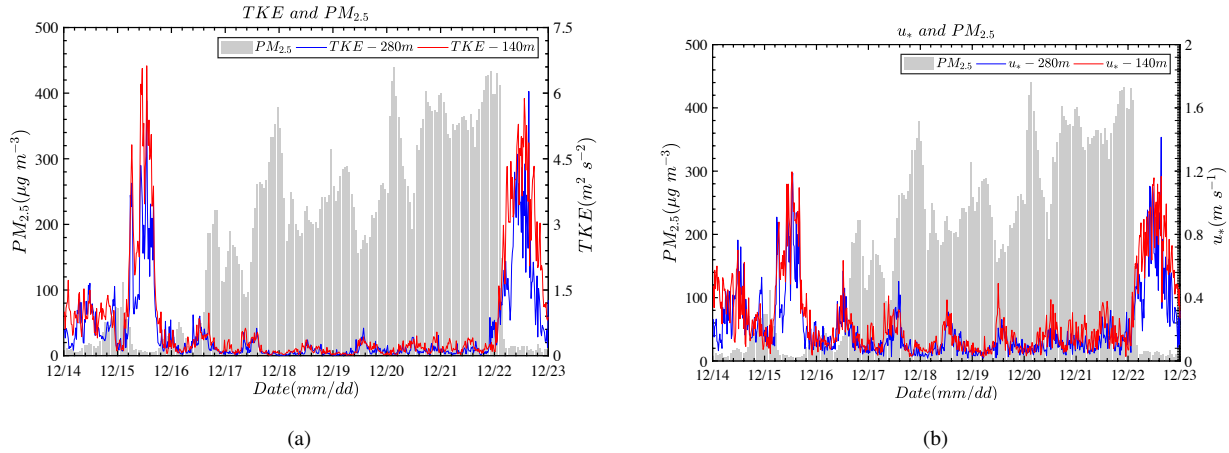
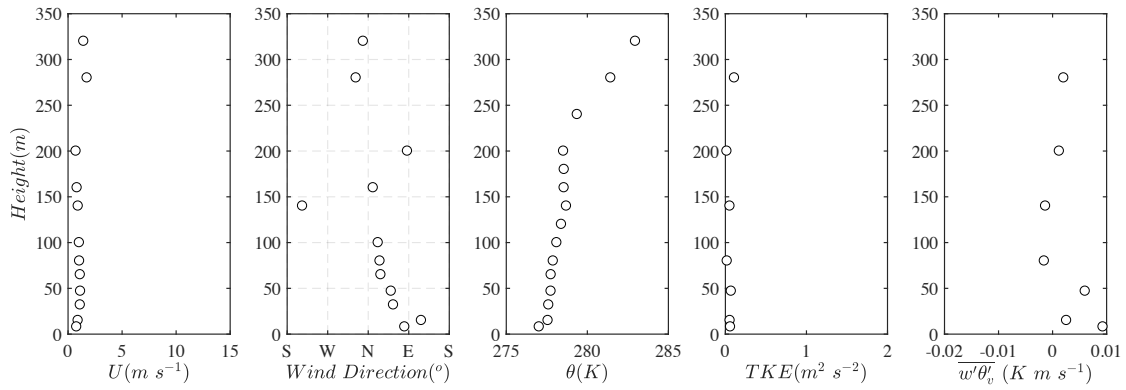
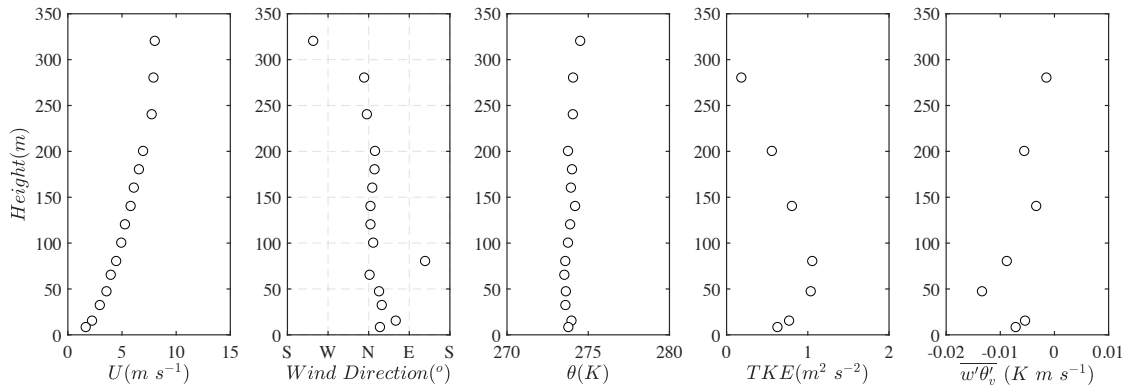


Figure 8. Time series of (a) turbulent kinetic energy ($m^2 s^{-2}$) and (b) friction velocity (u_* , $m s^{-1}$) at 140 m (red line) and 280 m (green line); $PM_{2.5}$ ($\mu g m^{-3}$) concentrations are also shown in the figures (grey column).

To understand the vertical structure characteristics of the ABL observed from the tower during the polluted and unpolluted
5 periods, profiles for wind, potential temperature (θ), TKE and sensible heat flux ($\overline{w'\theta'_v}$) for the lower boundary layer are also given. At night (see Fig.9), the wind speed profile for the clear day basically follows a logarithmic distribution and the potential temperature changes little from the ground to approximately 300 m. For turbulent values, TKE gradually decreased from approximately 70 m, and sensible heat flux was basically negative. On the polluted day, wind speeds from the lower
10 from the ground to approximately 200 m, indicating that the atmosphere basically maintained neutral levels of stratification. A pronounced inversion layer cap is also observed to approximately 200 m from the surface. TKE levels were basically maintained at close to zero. Note that at this time the sensible heat flux measured at above 80 m remained at close to zero. Close to the ground, sensible heat flux was slightly positive, demonstrating that when pollution occurred and especially when the inversion
15 and the weakening of turbulence ~~would aggravate the pollution situation~~ activities aggravated pollution levels once again.



(a)



(b)

Figure 9. Vertical profiles of wind speed (U), wind direction (WD), potential temperature (θ), turbulent kinetic energy (TKE) and sensible heat flux ($\overline{w'\theta'_v}$) at 23:20 on 19 December, 2016 (a), 22 December, 2016 (b).

In the daytime on 21 December 2016 (see Fig. 10), the $PM_{2.5}$ concentrations reached roughly $400 \mu g m^{-3}$, wind speeds were low, TKE remained zero value, and the potential temperature observed from the tower during the period of pollution basically denoted neutral stratification. The sensible heat flux was positive, but the value was basically measured as $0.02 K m s^{-1}$. At noon on 22 December, when the weather had improved, wind speeds were clearly higher. TKE still reached a maximum at 47 m. The influence of the urban canopy was stronger at heights of below 47 m. Unlike on the polluted day, levels of sensible heat flux were higher at this time, and the lower layer reached a value of $0.1 K m s^{-1}$. The tower observation data clearly show that levels of sensible heat flux decreased significantly in the daytime during the haze episode because of the higher levels of solar radiation scattering by particles.

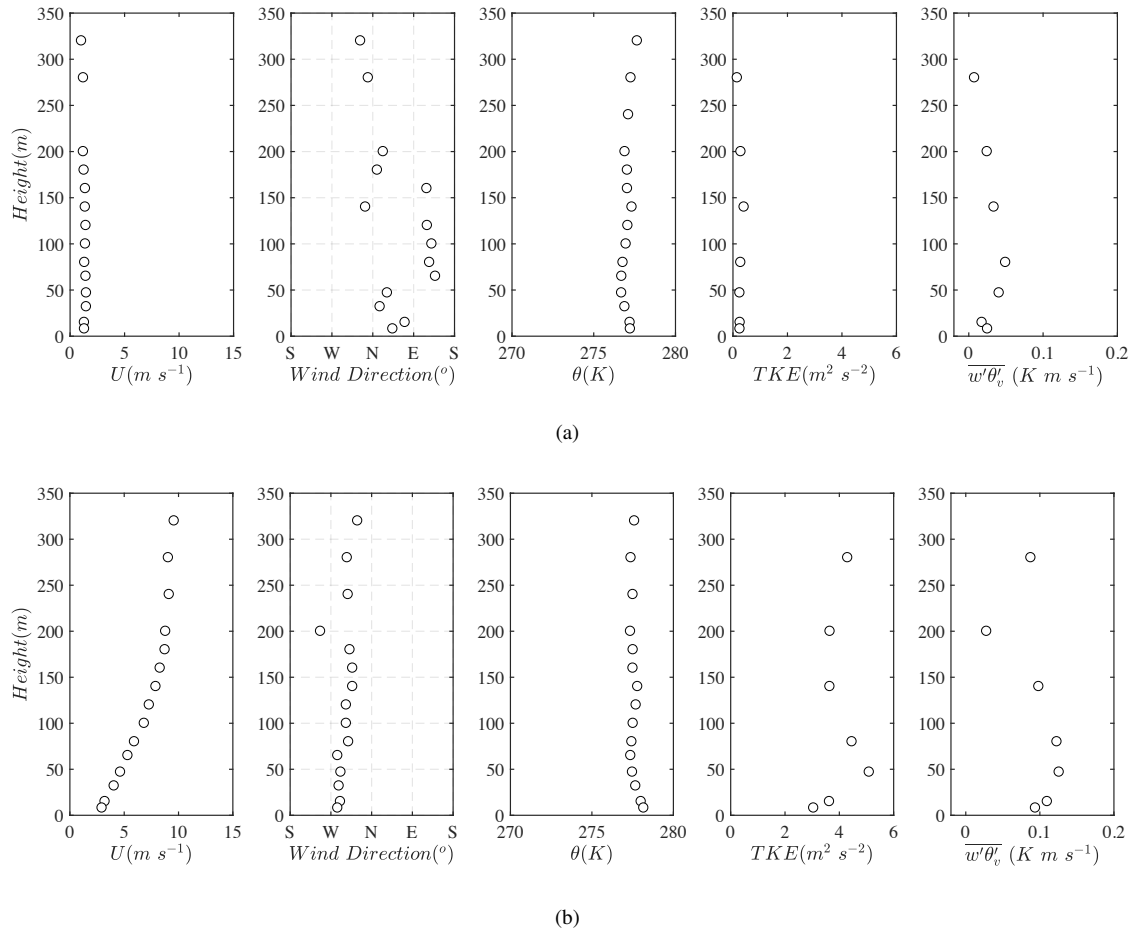


Figure 10. Vertical profiles of wind speed (U), wind direction (WD), potential temperature (θ), turbulent kinetic energy (TKE) and sensible heat flux ($\overline{w'\theta'_v}$) measured at 12:00 on 21 December, 2016 (a) and 22 December, 2016 (b).

According to the concentration of $PM_{2.5}$ observed, the haze pollution episode can be divided into different grades. Statistical mean values of surface visibility (Vis), wind speed (U), RH , ABL height and turbulent fluctuations are also calculated. As is shown in Table 2, the statistical averages further confirm the conclusions of the previous analysis. Rather, when the concentration of $PM_{2.5}$ is high, visibility and wind speed decrease while RH increases significantly. Our results show that due to the accumulation of aerosol particles, H_c is heightened slightly while H_c/H_u declines by roughly 300m. The Lidar results overestimate the ABL height at night (Quan et al., 2013). In this study the ABL height also increased due to the accumulation of pollutants during the period of heavy pollution. The turbulence levels observed also exhibit a decreasing trend occurring during the haze pollution episode, further demonstrating that turbulent activities are inhibited to a certain extent. We note that there appears to be only slight differences between the ABL height under slightly, moderately, heavily, and seriously polluted conditions. Since the data examined in this study apply to only one period of heavy pollution, the minor differences observed may not be statistically different across categories except when compared to “good” air quality conditions.

Table 2. Averaged values of visibility (Vis), wind speed (U), relative humidity (RH), ABL height (H_u , H_c), turbulent kinetic energy (TKE), friction velocity (u_*), momentum flux ($\overline{u'w'}$), and sensible heat flux ($\overline{w'\theta'_v}$) for different levels of pollution. Corresponding relationships between air pollution levels and $\text{PM}_{2.5}$ concentrations are as follows: good ($0\sim 75\mu\text{g m}^{-3}$), slightly polluted ($75\sim 115\mu\text{g m}^{-3}$), moderately polluted ($115\sim 150\mu\text{g m}^{-3}$), heavily polluted ($150\sim 250\mu\text{g m}^{-3}$), and seriously polluted ($>250\mu\text{g m}^{-3}$).

Quality Level	Vis (km)	U (m s^{-1})	RH (%)	TKE ($\text{m}^2 \text{s}^{-2}$)	u_* (m s^{-1})	$\overline{u'w'}$ ($\text{m}^2 \text{s}^{-2}$)	$\overline{w'\theta'_v}$ (K m s^{-1})	H_u (m)	H_c (m)
Good	9.9	4.0	39	1.23	0.31	0.08	0.0115	1124	358
Slightly	5.8	1.5	73	0.22	0.15	0.02	0.0022	837	484
Moderately	6.7	1.3	64	0.51	0.2	0.03	0.0032	750	502
Heavily	4.6	1.67	63	0.16	0.12	0.00045	0.0078	873	510
Seriously	2.0	1.38	81	0.15	0.11	0.0057	0.0038	844	518

4 Conclusions

In this paper a red warning haze pollution period running from 14 to 22 December 2016 occurring in Beijing was studied using various observational techniques. Atmospheric boundary layer structures and turbulence characteristics are the focus of this paper. Observational techniques used include not only remote sensing techniques, e.g., Lidar and WPR, but also direct measurement techniques, e.g., ground-based radiosonde technologies and the 325m meteorological tower. Our research results show that during the studied period of heavy haze pollution, the Beijing area was controlled by a stagnant weather system. Water vapor transport levels has increased relative humidity levels at below 600m, greatly promoting the hygroscopic growth of $PM_{2.5}$. The height of the ABL observed by Lidar (H_c) was measured at roughly 500~750m. ~~The inversion layer is closely related to the concentration of pollutants. Pollutants emitted in the ABL generally accumulate under the inversion layer. The inversion layer's height decreased significantly during the pollution period, and the lowest value was measured at below 500 m.~~ The present study shows that H_c did not seem to decline during the heavy pollution episode due to the accumulation of pollutants. According to the potential temperature gradient method, the ABL height calculated by radiosonde (H_θ) is in good agreement with H_c with a correlation coefficient of close to 72%. The ABL height (H_u) determined by WPR is higher than that of H_c , and H_u clearly decreased when heavy pollution levels of closer to H_c and H_θ occurred. Low TKE, u_* and $PM_{2.5}$ values were observed to be inversely related according to the tower data. ~~The turbulent fluxes varied very little with altitude, but the sensible heat flux was even slightly positive near the surface, indicating that the cooling effect is inhibited by the long-wave radiation from the ground.~~ Turbulent fluxes varied very little with altitude, but the sensible heat flux measured at night was slightly positive close to the Earth's surface, indicating that the cooling effect is inhibited by long-wave radiation from the ground. Due to higher levels of solar radiation scattering by particles, sensible heat flux in the daytime was greatly reduced. Consequently, the suppression of turbulence leads to more serious pollution outcomes.

Although different boundary layer heights can be obtained using various techniques, it seems that the ABL's height measured by Lidar can better reflect pollution levels that accumulate during periods of heavy haze pollution, and the ABL's height measured by radiosonde is also in good agreement with the H_c measured by Lidar, which is useful for the study of the atmospheric pollution boundary layer based on conventional observations. Our research importantly found that the ABL's height measured by WPR (H_u) is high. However, as the definition of ABL's height determined by different means varies within this class, they present respective roles and levels of significance. In our future work we will strive to parameterize the relationship between friction speed and $PM_{2.5}$ concentrations, as they exhibit strong statistical correlations (negative correlations) for use in numerical models of air pollution. In addition, it will be meaningful to explore the correlations between dynamic, thermal and material (concentration) boundary layer heights (expressed by H_u , H_θ and H_c , respectively) through more observations.

30 *Competing interests.* All the authors have declared that no competing interests exist

Acknowledgements. The authors thank Dr. Aiguo Li from the Institute of Atmospheric Physics of the Chinese Academy of Sciences for his assistance with the use of 325 m tower data. This work was supported by the National Key Research and Development Program of China (2017YFC0209605) and the National Natural Science Foundation of China (Grant No. 11472272).

References

- Al-Jiboori, M. H. and Fei, H.: Surface roughness around a 325-m meteorological tower and its effect on urban turbulence, *Advances in Atmospheric Sciences*, 22, 595–605, <https://doi.org/10.1007/BF02918491>, 2005.
- Allwine, K. J., Shinn, J. H., Streit, G. E., Clawson, K. L., and Brown, M.: OVERVIEW OF URBAN 2000 A Multiscale Field Study of
5 Dispersion through an Urban Environment, *Bulletin of the American Meteorological Society*, 83, 521–536, [https://doi.org/10.1175/1520-0477\(2002\)083<0521:OOUAMF>2.3.CO;2](https://doi.org/10.1175/1520-0477(2002)083<0521:OOUAMF>2.3.CO;2), 2002.
- Andreas, E. L., Claffey, K. J., and Makshtas, A. P.: Low-Level Atmospheric Jets And Inversions Over The Western Weddell Sea, *Boundary-Layer Meteorology*, 97, 459–486, <https://doi.org/10.1023/A:1002793831076>, 2000.
- Banta, R. M.: Stable-boundary-layer regimes from the perspective of the low-level jet, *Acta Geophysica*, 56, 58–87,
10 <https://doi.org/10.2478/s11600-007-0049-8>, 2008.
- Baumbach, G. and Vogt, U.: Influence of Inversion Layers on the Distribution of Air Pollutants in Urban Areas, *Water, Air, and Soil Pollution: Focus*, <https://doi.org/10.1023/A:1026098305581>, 2003.
- Bianco, L. and Wilczak, J. M.: Convective Boundary Layer Depth: Improved Measurement by Doppler Radar Wind Profiler Using Fuzzy Logic Methods, *Journal of Atmospheric and Oceanic Technology*, 19, 1745–1758, 2002.
- 15 Boers, R. and Eloranta, E. W.: Lidar measurements of the atmospheric entrainment zone and the potential temperature jump across the top of the mixed layer, *Boundary-Layer Meteorology*, 34, 357–375, <https://doi.org/10.1007/BF00120988>, 1986.
- Bravo-Aranda, J. A., de Arruda Moreira, G., Navas-Guzmán, F., Granados-Muñoz, M. J., Guerrero-Rascado, J. L., Pozo-Vázquez, D., Arbizu-Barrena, C., Reyes, F. J. O., Mallet, M., and Arboledas, L. A.: A new methodology for PBL height estimations based on lidar depolarization measurements: analysis and comparison against MWR and WRF model-based results, *Atmospheric Chemistry and Physics*, 17, 6839–
20 6851, <https://doi.org/10.5194/acp-17-6839-2017>, 2017.
- Brook, R. D., Franklin, B., Cascio, W., Hong, Y., Howard, G., Lipsett, M., Luepker, R., Mittleman, M., Samet, J., Smith, S. C., and Tager, I.: Air pollution and cardiovascular disease: A statement for healthcare professionals from the expert panel on population and prevention science of the American Heart Association, *Circulation*, 109, 2655–2671, <https://doi.org/10.1161/01.CIR.0000128587.30041.C8>, 2004.
- Brooks, I. M.: Finding Boundary Layer Top: Application of a Wavelet Covariance Transform to Lidar Backscatter Profiles, *Journal of
25 Atmospheric and Oceanic Technology*, 20, 1092–1105, [https://doi.org/10.1175/1520-0426\(2003\)020<1092:FBLTAO>2.0.CO;2](https://doi.org/10.1175/1520-0426(2003)020<1092:FBLTAO>2.0.CO;2), 2003.
- Cao, J. J., Lee, S. C., Ho, K. F., Zou, S. C., Fung, K., Li, Y., Watson, J. G., and Chow, J. C.: Spatial and seasonal variations of atmospheric organic carbon and elemental carbon in Pearl River Delta Region, China, *Atmospheric Environment*, 38, 4447–4456, <https://doi.org/10.1016/j.atmosenv.2004.05.016>, 2004.
- Chan, C. K. and Yao, X.: Air pollution in mega cities in China, *Atmospheric Environment*, 42, 1 – 42,
30 <https://doi.org/https://doi.org/10.1016/j.atmosenv.2007.09.003>, 2008.
- Chen, Y., An, J., Sun, Y., Wang, X., Qu, Y., Zhang, J., Wang, Z., and Duan, J.: Nocturnal Low-level Winds and Their Impacts on Particulate Matter over the Beijing Area, *Advances in Atmospheric Sciences*, 35, 1455–1468, <https://doi.org/10.1007/s00376-018-8022-9>, 2018.
- Chuang, P. Y.: Measurement of the timescale of hygroscopic growth for atmospheric aerosols, *Journal of Geophysical Research*, 108, <https://doi.org/10.1029/2002JD002757>, 2003.
- 35 Cohn, S. A. and Angevine, W. M.: Boundary Layer Height and Entrainment Zone Thickness Measured by Lidars and Wind-Profiling Radars., *Journal of Applied Meteorology*, 39, 1233–1247, [https://doi.org/10.1175/1520-0450\(2000\)039<1233:BLHAEZ>2.0.CO;2](https://doi.org/10.1175/1520-0450(2000)039<1233:BLHAEZ>2.0.CO;2), 2000.

- Davis, K. J., Gamage, N., Hagelberg, C. R., Kiemle, C., Lenschow, D. H., and Sullivan, P. P.: An Objective Method for Deriving Atmospheric Structure from Airborne Lidar Observations, *Journal of Atmospheric and Oceanic Technology*, 17, 1455–1468, <https://doi.org/10.1029/RG014i002p00215>, 2000.
- Devara, P. C. S., Raj, P. E., Murthy, B. S., Pandithurai, G., Sharma, S., and Vernekar, K. G.: Intercomparison of Nocturnal Lower-Atmospheric Structure Observed with Lidar and Sodar Techniques at Pune, India, *Journal of Applied Meteorology*, 34, 1375–1383, 1995.
- Ding, A. J., Fu, C. B., Yang, X. Q., Sun, J. N., Petäjä, T., Kerminen, V. M., Wang, T., Xie, Y., Herrmann, E., Herrmann, E., Zheng, L. F., Nie, W., Liu, Q., Wei, X. L., and Kulmala, M.: Intense atmospheric pollution modifies weather: a case of mixed biomass burning with fossil fuel combustion pollution in eastern China, *Atmospheric Chemistry and Physics*, 13, 10 545–10 554, <https://doi.org/10.5194/acpd-13-14377-2013>, 2013.
- 10 Ding, A. J., Huang, X., Nie, W., Sun, J. N., Kerminen, V., Petäjä, T., Su, H., Cheng, Y. F., Yang, X., Wang, M. H., Chi, X. G., Wang, J. P., Virkkula, A., Guo, W. D., Yuan, J., Wang, S. Y., Zhang, R. J., Wu, Y. F., Song, Y., Zhu, T., Zilitinkevich, S., Kulmala, M., and Fu, C. B.: Enhanced haze pollution by black carbon in megacities in China, *Geophysical Research Letters*, 43, 2873–2879, <https://doi.org/10.1002/2016GL067745>, 2016.
- Emeis, S. and Schäfer, K.: Remote Sensing Methods to Investigate Boundary-layer Structures relevant to Air Pollution in Cities, *Boundary-Layer Meteorology*, 121, 377–385, 2006.
- 15 Fisher, B., Kukkonen, J., and Schatzmann, M.: Meteorology applied to urban air pollution problems: COST 715, *International Journal of Environment and Pollution*, 16, 560–570, <https://doi.org/10.1504/IJEP.2001.000650>, 2001.
- Flamant, C., Pelon, J., Flamant, P. H., and Durand, P.: LIDAR DETERMINATION OF THE ENTRAINMENT ZONE THICKNESS AT THE TOP OF THE UNSTABLE MARINE ATMOSPHERIC BOUNDARY LAYER, *Boundary-Layer Meteorology*, 83, 247–284, <https://doi.org/10.5194/acpd-13-14377-2013>, 1997.
- 20 Fu, Q., Zhuang, G., Wang, J., Xu, C., Huang, K., Li, J., Hou, B., Lu, T., and Streets, D. G.: Mechanism of formation of the heaviest pollution episode ever recorded in the Yangtze River Delta, China, *Atmospheric Environment*, 42, 2023–2036, <https://doi.org/10.1016/j.atmosenv.2007.12.002>, 2008.
- Gao, Y., Zhang, M., Liu, Z., Wang, L., Wang, P., Xia, X., Tao, M., and Zhu, L.: Modeling the feedback between aerosol and meteorological variables in the atmospheric boundary layer during a severe fog-haze event over the North China Plain, *Atmospheric Chemistry and Physics*, 15, 1093–1130, <https://doi.org/10.5194/acp-15-4279-2015>, 2015.
- 25 Geiß, A., Wiegner, M., Bonn, B., Schäfer, K., and Nothard, R.: Mixing layer height as an indicator for urban air quality?, *Atmospheric Measurement Techniques*, 10, 2969–2988, 2017.
- Grimsdell, A. W. and Angevine, W. M.: Convective Boundary Layer Height Measurement with Wind Profilers and Comparison to Cloud Base, *Journal of Atmospheric and Oceanic Technology*, 15, 1331, [https://doi.org/10.1175/1520-0426\(1998\)015<1331:CBLHMW>2.0.CO;2](https://doi.org/10.1175/1520-0426(1998)015<1331:CBLHMW>2.0.CO;2), 1998.
- 30 Guo, X., Sun, Y., and Miao, S.: Characterizing Urban Turbulence Under Haze Pollution: Insights into Temperature–Humidity Dissimilarity, *Boundary-Layer Meteorology*, 158, 501–510, <https://doi.org/10.1007/s10546-015-0104-y>, 2016.
- Han, S., Liu, J., Hao, T., Zhang, Y., Li, P., Yang, J., Wang, Q., Cai, Z., Yao, Q., Zhang, M., and Wang, X.: Boundary layer structure and scavenging effect during a typical winter haze-fog episode in a core city of BTH region, China, *Atmospheric Environment*, 179, 187–200, <https://doi.org/10.1016/j.atmosenv.2018.02.023>, 2018.
- 35 Hennemuth, B. and Lammert, A.: Determination of the Atmospheric Boundary Layer Height from Radiosonde and Lidar Backscatter, *Boundary-Layer Meteorology*, 120, 181–200, <https://doi.org/10.1007/s10546-005-9035-3>, 2006.

- Hooper, W. P. and Eloranta, E. W.: Lidar Measurements of Wind in the Planetary Boundary Layer: The Method, Accuracy and Results from Joint Measurements with Radiosonde and Kytöön., *Journal of Applied Meteorology*, 25, 990–1001, [https://doi.org/10.1175/1520-0450\(1986\)025<0990:LMOWIT>2.0.CO;2](https://doi.org/10.1175/1520-0450(1986)025<0990:LMOWIT>2.0.CO;2), 1986.
- Hu, Xiaoming, Liu, Shuhua, Wang, Yingchun, Li, and Ju: Numerical Simulation of Wind and Temperature Fields over Beijing Area in Summer, *Journal of Meteorological Research*, pp. 120–127, 2005.
- Huang, R.-J., Zhang, Y., Bozzetti, C., Ho, K.-F., Cao, J.-J., Han, Y., Daellenbach, K. R., Slowik, J. G., Platt, S. M., Canonaco, F., Zotter, P., Wolf, R., Pieber, S. M., Bruns, E. A., Crippa, M., Ciarelli, G., Piazzalunga, A., Schwikowski, M., Ulcin Abbazade, G., Zimmermann, R., Onke Szidat, S., Baltensperger, U., Haddad, I. E., and Prevot, H.: High secondary aerosol contribution to particulate pollution during haze events in China, *Nature*, 514, 218–222, <https://doi.org/10.1038/nature13774>, 2014.
- 10 Jiannong, Quan, Yang, Qiang, Zhang, Xuexi, Junji, Suqin, Junwang, and Meng: Evolution of planetary boundary layer under different weather conditions, and its impact on aerosol concentrations, *Particuology*, 11, 34–40, <https://doi.org/10.1016/j.partic.2012.04.005>, 2013.
- Jong, S. A. P. D., Slingerland, J. D., and Giesen, N. C. V. D.: Fiber optic distributed temperature sensing for the determination of air temperature, *Atmospheric Measurement Techniques*, 8, 1(2015-01-15), 7, 335–339, 2015.
- Kalapureddy, M. C. R., Rao, D. N., Jain, A. R., and Ohno, Y.: Wind profiler observations of a monsoon low-level jet over a tropical Indian station, *Annales Geophysicae*, 25, 2125–2137, <https://doi.org/10.5194/angeo-25-2125-2007>, 2007.
- 15 Katul, G., Goltz, S. M., Hsieh, C.-I., Cheng, Y., Mowry, F., and Sigmon, J.: Estimation of surface heat and momentum fluxes using the flux-variance method above uniform and non-uniform terrain, *Boundary-Layer Meteorology*, 74, 237–260, <https://doi.org/10.1007/BF00712120>, 1995.
- Keller, C. A., Huwald, H., Vollmer, M. K., Wenger, A., Hill, M., Parlange, M. B., and Reimann, S.: Fiber optic distributed temperature sensing for the determination of the nocturnal atmospheric boundary layer height, *Atmospheric Measurement Techniques*, 4, 143–149, 2010.
- Lance, S., Raatikainen, T., Onasch, T. B., Worsnop, D. R., Yu, X. Y., Alexander, M. L., Stolzenburg, M. R., McMurry, P. H., Smith, J. N., and Nenes, A.: Aerosol mixing state, hygroscopic growth and cloud activation efficiency during MIRAGE 2006, *Atmospheric Chemistry and Physics*, 13, 5049–5062, <https://doi.org/10.5194/acp-13-5049-2013>, 2012.
- 25 Li, J., Fu, Q., Huo, J., Wang, D., Yang, W., Bian, Q., Duan, Y., Zhang, Y., Pan, J., and Lin, Y.: Tethered balloon-based black carbon profiles within the lower troposphere of Shanghai in the 2013 East China smog, *Atmospheric Environment*, 123, 327–338, <https://doi.org/10.1016/j.atmosenv.2015.08.096>, 2015.
- Li, J., Sun, J., Zhou, M., Cheng, Z., Li, Q., Cao, X., and Zhang, J.: Observational analyses of dramatic developments of a severe air pollution event in the Beijing area, *Atmospheric Chemistry and Physics*, 18, 3919–3935, <https://doi.org/10.5194/acp-18-3919-2018>, 2017.
- 30 Liang, X., Miao, S., Li, J., Bornstein, R., Zhang, X., Gao, Y., Cao, X., Chen, F., Cheng, Z., Clements, C., Dabberdt, W., Ding, A., Ding, D., Dou, J. J., Dou, J. X., Dou, Y., Grimmond, C. S. B., Gonzalez-Cruz, J., He, J., Huang, M., Huang, X., Ju, S., Li, Q., Niyogi, D., Quan, J., Sun, J., Sun, J. Z., Yu, M., Zhang, J., Zhang, Y., Zhao, X., Zheng, Z., and Zhou, M.: SURF: Understanding and Predicting Urban Convection and Haze, *Bulletin of the American Meteorological Society*, <https://doi.org/10.1175/BAMS-D-16-0178.1>, 2018.
- Liu, X., Zhang, Y., Cheng, Y., Hu, M., and Han, T.: Aerosol hygroscopicity and its impact on atmospheric visibility and radiative forcing in Guangzhou during the 2006 PRIDE-PRD campaign, *Atmospheric Environment*, 60, 59–67, <https://doi.org/10.1016/j.atmosenv.2012.06.016>, 2012.
- Martucci, G., Matthey, R., Mitev, V., and Richner, H.: Comparison between Backscatter Lidar and Radiosonde Measurements of the Diurnal and Nocturnal Stratification in the Lower Troposphere, *Journal of Atmospheric Oceanic Technology*, 24, 1158–1164, 2006.

- Miao, Y., Guo, J., Liu, S., Zhao, C., Li, X., Zhang, G., Wei, W., and Ma, Y.: Impacts of synoptic condition and planetary boundary layer structure on the trans-boundary aerosol transport from Beijing-Tianjin-Hebei region to northeast China, *Atmospheric Environment*, 181, 1–11, <https://doi.org/10.1016/j.atmosenv.2018.03.005>, 2018.
- 5 Pan, X. L., Yan, P., Tang, J., Ma, J. Z., Wang, Z. F., Gbaguidi, A., and Sun, Y. L.: Observational study of influence of aerosol hygroscopic growth on scattering coefficient over rural area near Beijing mega-city, *Atmospheric Chemistry and Physics*, 9, 7519–7530, <https://doi.org/10.5194/acp-9-7519-2009>, 2009.
- Pichugina, Y. L. and Banta, R. M.: Stable Boundary Layer Depth from High-Resolution Measurements of the Mean Wind Profile, *Journal of Applied Meteorology and Climatology*, 49, 20–35, <https://doi.org/10.1175/2009JAMC2168.1>, 2010.
- 10 Quan, J., Yang, G., Qiang, Z., Tie, X., Cao, J., Han, S., Meng, J., Chen, P., and Zhao, D.: Evolution of planetary boundary layer under different weather conditions, and its impact on aerosol concentrations, *Particuology*, 11, 34–40, 2013.
- Quan, L. and Hu, F.: Relationship between turbulent flux and variance in the urban canopy, *Meteorology and Atmospheric Physics*, 104, 29–36, <https://doi.org/10.1007/s00703-008-0012-5>, 2009.
- Ren, Y., Zheng, S., Wei, W., Wu, B., Zhang, H., Cai, X., and Song, Y.: Characteristics of Turbulent Transfer during Episodes of Heavy Haze Pollution in Beijing in Winter 2016/17, *Journal of Meteorological Research*, 32, 69–80, <https://doi.org/10.1007/s13351-018-7072-3>, 2018.
- 15 Schäfer, K., Emeis, S., Hoffmann, H., and Jahn, C.: Influence of mixing layer height upon air pollution in urban and sub-urban areas, *Meteorologische Zeitschrift*, 15, 647–658, 2006.
- Seibert, P., Beyrich, F., Gryning, S. E., Joffre, S., Rasmussen, A., and Tercier, P.: Review and intercomparison of operational methods for the determination of the mixing height, *Atmospheric Environment*, 34, 1001–1027, [https://doi.org/10.1016/S1352-2310\(99\)00349-0](https://doi.org/10.1016/S1352-2310(99)00349-0), 2000.
- Seinfeld, J. H. and Pandis, S. N.: *Atmospheric Chemistry and Physics: From Air Pollution to Climate Change*, 1997.
- 20 Sheng, J., Zhao, D., Ding, D., Li, X., Huang, M., Gao, Y., Quan, J., and Zhang, Q.: Characterizing the level, photochemical reactivity, emission, and source contribution of the volatile organic compounds based on PTR-TOF-MS during winter haze period in Beijing, China, *Atmospheric Research*, 212, <https://doi.org/10.1016/j.atmosres.2018.05.005>, 2018.
- Sorbjan, Z.: *Structure of the Atmospheric boundary layer*, Prentice Hall, Englewood Cliffs, N.J., 1989.
- Stull, R. B.: *An Introduction to Boundary Layer Meteorology*, Atmospheric Sciences Library, 8, 89, 1988.
- 25 Summa, D., Girolamo, P. D., Stelitano, D., and Cacciani, M.: Characterization of the planetary boundary layer height and structure by Raman lidar: comparison of different approaches, *Atmospheric Measurement Techniques*, 6, 3515–3525, <https://doi.org/10.5194/amt-6-3515-2013>, 2013.
- Sun, Y., Zhuang, G., Tang, A., Wang, Y., and An, Z.: Chemical characteristics of PM_{2.5} and PM₁₀ in haze-fog episodes in Beijing., *Environmental Science and Technology*, 40, 3148–3155, <https://doi.org/10.1021/es051533g>, 2006.
- 30 Sun, Y., Jiang, Q., Wang, Z., Fu, P., Li, J., Yang, T., and Yin, Y.: Investigation of the sources and evolution processes of severe haze pollution in Beijing in January 2013, *Journal of Geophysical Research*, 119, 4380–4398, <https://doi.org/10.1002/2014JD021641>, 2014.
- Sun, Y., Du, W., Wang, Q., Zhang, Q., Chen, C., Chen, Y., Chen, Z., Fu, P., Wang, Z., Gao, Z., and Worsnop, D. R.: Real-Time Characterization of Aerosol Particle Composition above the Urban Canopy in Beijing: Insights into the Interactions between the Atmospheric Boundary Layer and Aerosol Chemistry., *Environmental Science and Technology*, 49, 11 340–11 347, <https://doi.org/10.1021/acs.est.5b02373>, 2015.
- 35 Sun, Y. L., Wang, Z. F., Fu, P. Q., Yang, T., Jiang, Q., Jiang, Q., Dong, H. B., Li, J., and Jia, J. J.: Aerosol composition, sources and processes during wintertime in Beijing, China, *Atmospheric Chemistry and Physics*, 13, 4577–4592, <https://doi.org/10.5194/acp-13-4577-2013>, 2013.

- Svenningsson, I. B., Hansson, H.-C., Wiedensohler, A., Ogren, J. A., Noone, K. J., and Hallberg, A.: Hygroscopic growth of aerosol particles in the Po Valley, *Tellus B*, 44, 556–569, 1992.
- Wang, H., Wang, H., Xue, M., Zhang, X. Y., Liu, H. L., Zhou, C. H., Tan, S. C., Che, H. Z., Chen, B., and Li, T.: Mesoscale modeling study of the interactions between aerosols and PBL meteorology during a haze episode in Jing–Jin–Ji (China) and its nearby surrounding region – Part 1: Aerosol distributions and meteorological features, *Atmospheric Chemistry and Physics*, 15, 3257–3275, <https://doi.org/10.5194/acp-15-3257-2015>, 2014b.
- Wang, Q., Sun, Y., Xu, W., Du, W., Zhou, L., Tang, G., Chen, C., Cheng, X., Zhao, X., and Ji, D.: Vertically resolved characteristics of air pollution during two severe winter haze episodes in urban Beijing, China, *Atmospheric Chemistry and Physics*, 18, 1–28, <https://doi.org/10.5194/acp-18-2495-2018>, 2018.
- 10 Wang, Y., Klipp, C. L., Garvey, D. M., Ligon, D. A., Williamson, C. C., Chang, S. S., Newsom, R. K., and Calhoun, R.: Nocturnal Low-Level-Jet-Dominated Atmospheric Boundary Layer Observed by a Doppler Lidar Over Oklahoma City during JU2003, *Journal of Applied Meteorology and Climatology*, 46, 2098–2109, <https://doi.org/10.1175/2006JAMC1283.1>, 2007.
- Wang, Y. S., Li, Y., Wang, L. L., Liu, Z. R., Dongsheng, J. I., Tang, G. Q., Zhang, J. K., Yang, S., Bo, H. U., and Xin, J. Y.: Mechanism for the formation of the January 2013 heavy haze pollution episode over central and eastern China, *Science China Earth Sciences*, 57, 14–25, <https://doi.org/10.1007/s11430-013-4773-4>, 2014a.
- 15 Wang, Z., Wang, Z., Cao, X., Zhang, L., Notholt, J., Zhou, B., Liu, R., and Zhang, B.: Lidar measurement of planetary boundary layer height and comparison with microwave profiling radiometer observation, *Atmospheric Measurement Techniques*, 5, 1965–1972, <https://doi.org/10.5194/amtd-5-1233-2012>, 2012.
- Wei, W., Zhang, H., Wu, B., Huang, Y., Cai, X., Song, Y., and Li, J.: Intermittent turbulence contributes to vertical diffusion of PM_{2.5} in the North China Plain, *Atmospheric Chemistry and Physics*, pp. 1–21, <https://doi.org/10.5194/acp-18-12953-2018>, 2018.
- Zhang, Q., Quan, J., Tie, X., Li, X., Liu, Q., Gao, Y., and Zhao, D.: Effects of meteorology and secondary particle formation on visibility during heavy haze events in Beijing, China, *Science of The Total Environment*, 502, 578–584, <https://doi.org/10.1016/j.scitotenv.2014.09.079>, 2015b.
- Zhang, R., Wang, G., Guo, S., Zamora, M. L., Ying, Q., Lin, Y., Wang, W., Hu, M., and Wang, Y.: Formation of Urban Fine Particulate Matter, *Chemical Reviews*, 115, 3803–3855, <https://doi.org/10.1021/acs.chemrev.5b00067>, 2015a.
- 25 Zhang, X. Y., Wang, Y. Q., Niu, T., Zhang, X. C., Gong, S. L., Zhang, Y. M., and Sun, J. Y.: Atmospheric aerosol compositions in China: spatial/temporal variability, chemical signature, regional haze distribution and comparisons with global aerosols, *Atmospheric Chemistry and Physics*, 12, 779–799, <https://doi.org/10.5194/acp-12-779-2012>, 2011.